AD-A162 388 INVESTIGATION OF RUBIDIUM HYPERFINE STRUCTURE FREQUENCY STABILIZATION MEC (U) LITTON SYSTEMS INC WOODLAND HILLS CA GUIDANCE AND CONTROL SYS 1/1

UNCLASSIFIED T MCCLELLAND ET AL AUG 84 AFOSR-TR-85-1103 F/G 14/2 NL

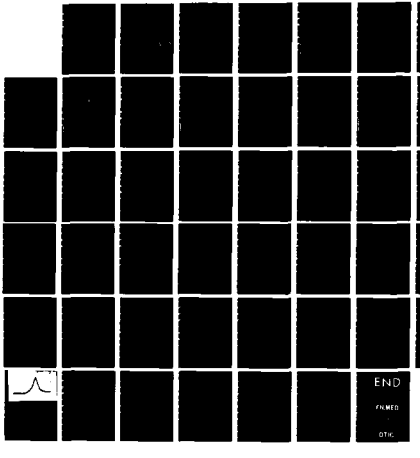

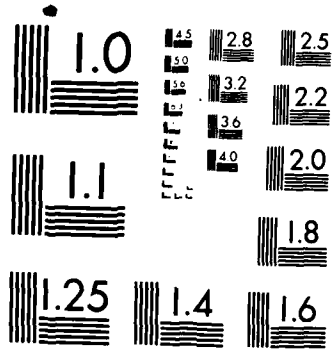

UNCLASSIFIED

SECURITY CLASSIFICATION OF THIS PAGE (When Data Entered)

(2)

REPORT DOCUMENTATION PAGE		READ INSTRUCTIONS BEFORE COMPLETING FORM
1 REPORT NUMBER AFOSR-TR- 193	2 GOVT ACCESSION NO.	3 RECIPIENT'S CATALOG NUMBER
4 TITLE (and Subtitle) Investigation of Rubidium Hyperfine Structure Frequency Stabilization Mechanisms		5 TYPE OF REPORT & PERIOD COVERED Final (August 1983 to July 1984)
		6 PERFORMING ORG. REPORT NUMBER
7 AUTHOR(s) T. McClelland, T.M. Kwon		8 CONTRACT OR GRANT NUMBER(s) F49620-83-C-0132
9 PERFORMING ORGANIZATION NAME AND ADDRESS Litton Guidance and Control Systems 5500 Canoga Avenue Woodland Hills, California 91365		10 PROGRAM ELEMENT PROJECT, TASK AREA & WORK UNIT NUMBERS 61102F 2301/A4
11 CONTROLLING OFFICE NAME AND ADDRESS Director of Physics Code FQ 8671 Air Force Office of Scientific Research Attn: NP Bldg. 410, Bolling AFB, DC 20332		12 REPORT DATE August 1984
		13 NUMBER OF PAGES
14 MONITORING AGENCY NAME & ADDRESS(if different from Controlling Office)		15 SECURITY CLASS. (of this report) UNCLASSIFIED
		15a DECLASSIFICATION/DOWNGRADING SCHEDULE

16 DISTRIBUTION STATEMENT (of this Report)

Approved for public release; distribution unlimited.

17 DISTRIBUTION STATEMENT (of the abstract entered in Block 20, if different from Report)

DTIC ELECTE DEC 09 1985 S D

18 SUPPLEMENTARY NOTES

19 KEY WORDS (Continue on reverse side if necessary and identify by block number)

Optical Pumping
Rubidium
Frequency Standard
Frequnecy Shift
Light Shift
Density Matrix
Buffer Gas
Linewidth
Magnetic Resonance

20 ABSTRACT (Continue on reverse side if necessary and identify by block number)

The linewidth and frequency associated with the ground state hyperfine energy of Rb^{87} has been studied. A stable single mode semiconductor laser is used to optically pump Rb, in order to obtain a highly collimated, monochromatic light source. The laser is stabilized by locking its optical

DD FORM 1 JAN 73 1473 EDITION OF 1 NOV 65 IS OBSOLETE S/N 0102-014-6601

UNCLASSIFIED

SECURITY CLASSIFICATION OF THIS PAGE (When Data Entered)

AD-A162 388

DTIC FILE COPY

frequency to the Rb absorption line center. The dependence of the hyperfine frequency and resonance linewidth have been measured as a function of temperature, light intensity and microwave power; and a theoretical description of the linewidth vs. temperature data is presented.

TABLE OF CONTENTS

TABLE OF CONTENTS

LIST OF ILLUSTRATIONS

LIST OF TABLES

SECTION I

PROGRAM DESCRIPTION

1.1 INTRODUCTION

It is the goal of this research to understand the physics related to the ground state hyperfine level separation in Rb^{87}; with sufficient precision to predict effects as small as 10^{-11} of this separation. The work reported herein represents a continuation of work begun in 1982, and reported on in 1983.[1] A more complete description of the program goals, as well as the initial findings, can be found in the 1983 report.

In order to understand in detail the physics associated with measurement of the hyperfine frequency of Rb^{87}, it has been determined that a very monochromatic light source is necessary.[1] If carefully used, a semiconductor laser provides just such a light source, and hence this research incorporates a laser of this type to make measurements.

The design and implementation of apparatus capable of making the desired measurements is described in Section II of this report. Special considerations necessary to utilize lasers in this application are noted.

In Section III the experimental results are discussed. Special emphasis is given to measurement of hyperfine magnetic resonance linewidth as a function of temperature, as the results of these measurements are contrary to previous predictions. These measurements, and a theoretical description are detailed in Appendix A, which is a self-contained manuscript submitted for publication.

The results of this research are summarized in Section IV.

1.2 ACKNOWLEDGEMENTS

The authors are indebted to a number of people at Litton who have contributed to this project. In particular, we thank Dr. Leo Lam for his physical insight and many illuminating discussions, and Mr. William Debley for his general laboratory support. We also thank Mr. Charles Quinn for design and fabrication of much of the laser diode stabilization circuitry.

All the progress we have made at Litton has been through the encouragement and funding provided by AFOSR. The program manager has been Dr. Ralph Kelley.

SECTION II

LASER DIODE ENGINEERING

2.1 GENERAL

Although the use of a laser light source with a narrow, well defined spectral profile in principle greatly simplifies the interpretation of experimental data, the light frequency must be stabilized to great precision in order to realize this simplification. This becomes clear when it is realized that laser diode frequency fluctuation of 1 MHz can easily cause frequency fluctuations of $\sim 1 \times 10^{-10}$ in a Rb frequency standard.

The ground state hyperfine energy separation of Rb is light shifted by resonant light by an amount proportional to the light intensity; but also dependent on the light frequency, as shown in Figure 2-1. Since the absorption peaks (see Figure 2-1) for Rb resonant light correspond to the regions of greatest slope of the light shift curves, it is clear that relatively small frequency fluctuations in a laser tuned to an absorption line center produce relatively large frequency shifts.

It was decided for this effort that useful information could only be obtained if short term light induced frequency fluctuations could be kept below the level of 1×10^{-10}; corresponding to

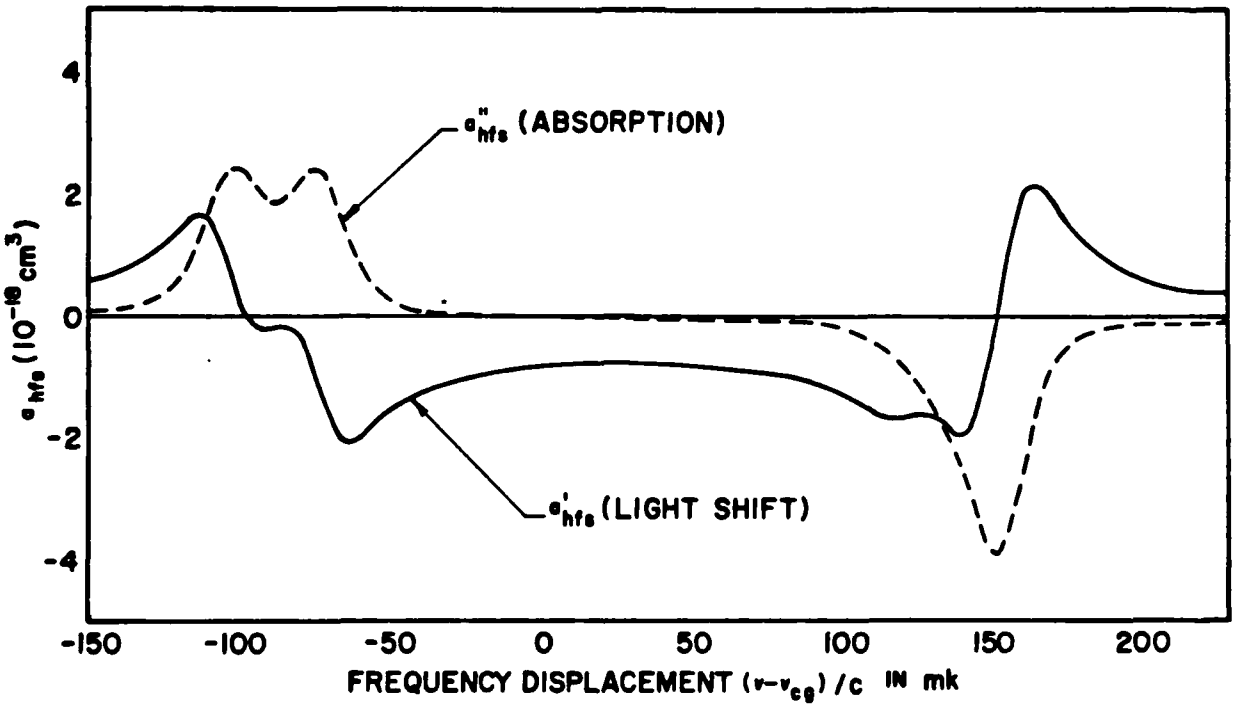

FIG. 2-1

D_1 ABSORPTION AND LIGHT SHIFT FOR Rb^{87} DUE TO HYPERFINE POLARIZABILITY

laser stability of $\leq$ 1 MHz. The laser diodes used had emission linewidths of $\sim$100 MHz, so this means stabilizing the line center to 1% of the linewidth.

Laser diode output frequency is affected primarily by the temperature of the P-N junction for the operating levels of interest. However, junction temperature is extremely dependent on forward bias current, as well as ambient temperature. Thus both bias current and heat sink temperature must be stabilized sufficiently to keep light fluctuations below the 1 MHz level. The sensitivities of the commercially available lasers used in this work are shown in Table 2-1. From the table it is clear that laser diode current must be stabilized to $\sim 1 \times 10^{-5}$, and temperature to $\sim 1 \times 10^{-4}$°C, for a passively stabilized laser diode.

2.2 LASER FREQUENCY STABILIZATION

It was decided that the best way to obtain the necesary frequency stability was to lock the laser light output to the Rb absorption line. A block diagram of the apparatus developed for this purpose is shown in Figure 2-2. With this apparatus, LD frequency was locked with an accuracy of better than 1 MHz (limit of measurement sensitivity), with a loop time constant of $\sim$1 sec.

TABLE 1

EXPERIMENTALLY MEASURED LASER PARAMETERS

LASER DIODE		FORWARD BIAS CURRENT, I		$\frac{\partial f}{\partial I}\ T=T_o$	$I\ \frac{\partial f}{\partial I}$	$\frac{\partial f}{\partial T}\ I=I_o$	LIGHT AMPLITUDE, A, (mW)	
MANUFACTURER	MODEL NO.	I(mA)	$\frac{\partial I}{\partial T}\ f=D_1$ (mA/°C)	(GHz/ mA)	(GHz)	(GHz/mA)	A (mW)	$\frac{\partial A}{\partial T}\ f=D_1$ (mW/°C)
Mitsubishi	3301	22	N/A	7.5	165	28	3	N/A
Mitsubishi	4101	22	N/A	9.0	198	N/A	3	N/A
Hitachi	7801	50	-8.9	3.3	165	N/A	4	3

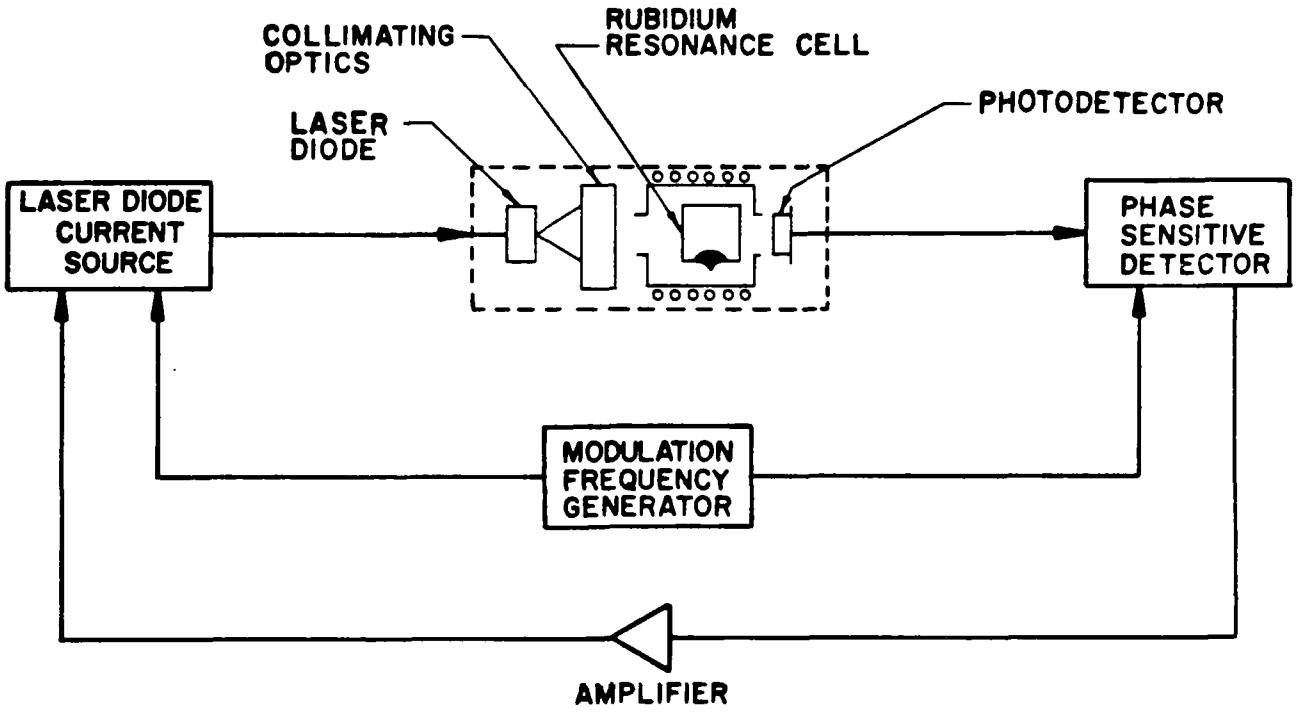

FIG. 2-2

LASER DIODE ACTIVE STABILIZATION

2.3 LASER TEMPERATURE STABILIZATION

By actively locking LD frequency to the Rb absorption, sensitivity to temperature fluctuations is greatly reduced. However, changes in ambient temperature result in an error signal to the current controller, which then corrects the current in order to maintain constant frequency. Referring to Figure 2-1, and the last column of Table 2-1, it is clear that the temperature drifts of the laser diode heat sink can cause unacceptable Rb frequency shifts.

The necessary temperature stability can be obtained for short periods of time ($\sim$ minutes) with standard thermo-electric controllers; as long as the thermal mass to which the diode is heat-sunk is large enough. A diagram of the heat-sink/TE oven used in this work is shown in Figure 2-3. The temperature was controlled by feeding back the voltage, developed across a platinum, temperature sensitive resistor attached to the laser diode heat sink, to the TE oven current control. By surrounding the diode with thermally insulating glass wool, and minimizing ambient convection currents, it was possible to obtain .01°C temperature stability for periods of $\sim$10 mins. Over longer periods of time, temperature drifts of $\sim$0.2°C were observed.

2.4 LASER LIGHT OUTPUT

In order to unambiguously interpret measurements it is desirable to have a perfectly collimated light source with a well defined beam profile.

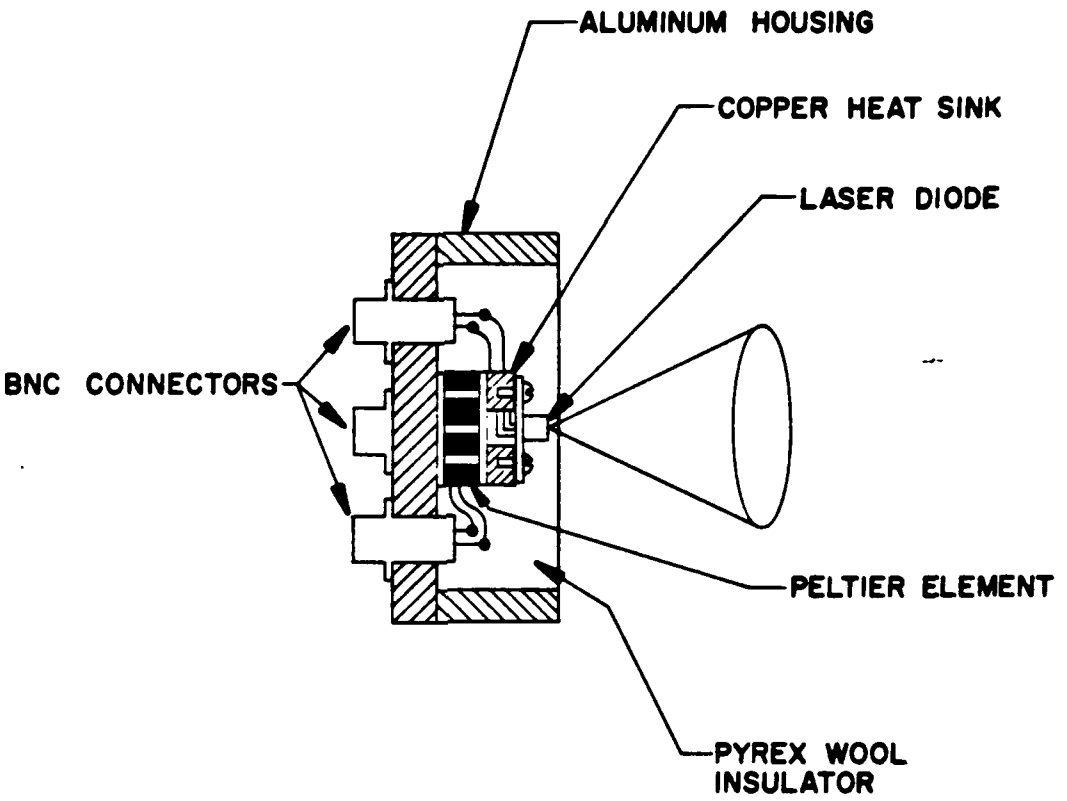

FIG.2-3

CROSS-SECTION OF LASER DIODE PELTIER TEMPERATURE CONTROL UNIT

Collimation of the laser diode output is in principle quite simple since the beam diverges from a region with dimensions of $\sim 1\mu m$. In reality some slight astigmatism is usually observed in the output, however, for the laser diodes used in this work, the astigmatism is quite small. The divergence of the beam after collimation was observed to be very small. Figure 2-4 shows the beam profile for two different distances from the collimating optics, measured along a horizontal axis. Also shown in the figure is a gaussian curve of approximately the same width.

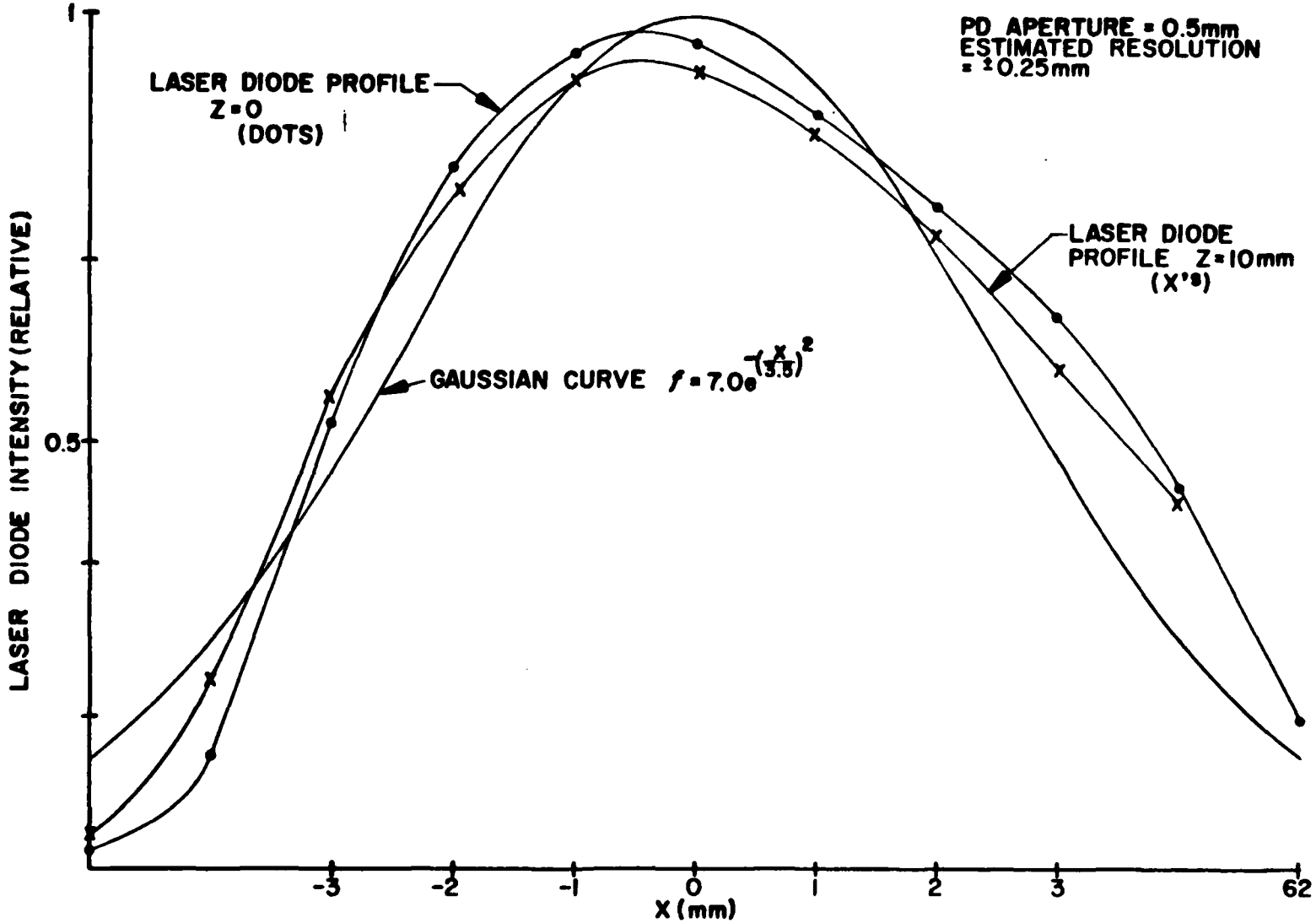

(FIG.2-4) LASER DIODE PROFILE

SECTION III

EXPERIMENTAL RESULTS

3.1 GENERAL

A schematic diagram of the experimental apparatus used to make measurements is shown in Figure 3-1. An actively stabilized laser, as described in Section II, is used to optically pump Rb^{87} atoms confined to a cell inside a microwave cavity. The microwave cavity resonates at the m=0→m-0 resonant frequency of Rb^{87}, and by tuning the frequency of the field applied to the cavity, the Rb^{87} resonance can be studied. More details of this configuration are given in the Annual Report for last year.[1]

The frequency synthesizer can be either phase modulated or amplitude modulated. When amplitude modulated, the signal output from the phase sensitive detector, as a function of synthesizer frequency, gives the Rb^{87} microwave absorption curve. When phase modulated, the signal output as a function of synthesizer frequency gives an error signal. For small modulation amplitudes (compared to the absorption linewidth) this error signal is the derivative of the absorption signal. These signals are shown, for typical measurement conditions, in Figure 3-2.

Numerous measurements of the dependence of resonant frequency and linewidth on external parameters have been made. External

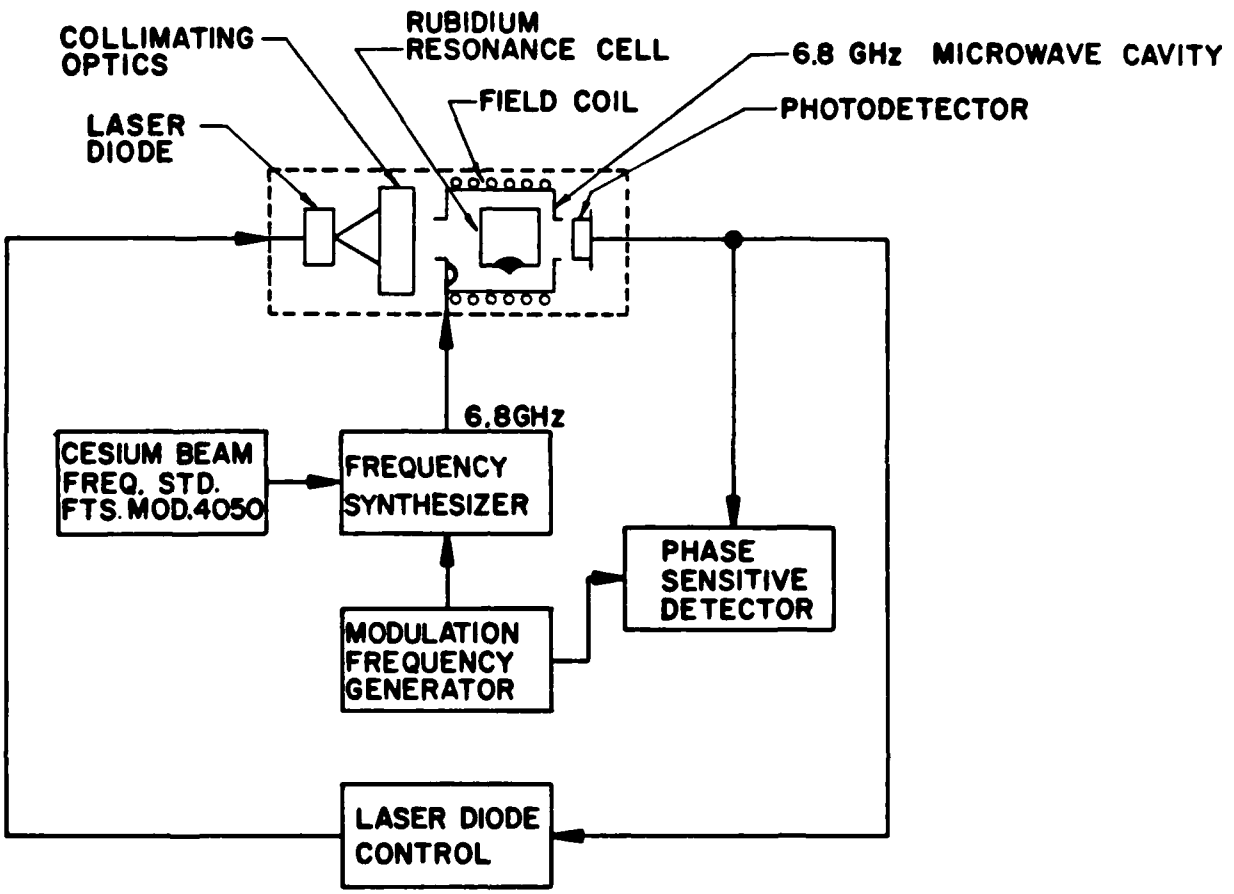

FIG. 3-1

EXPERIMENTAL APPARATUS

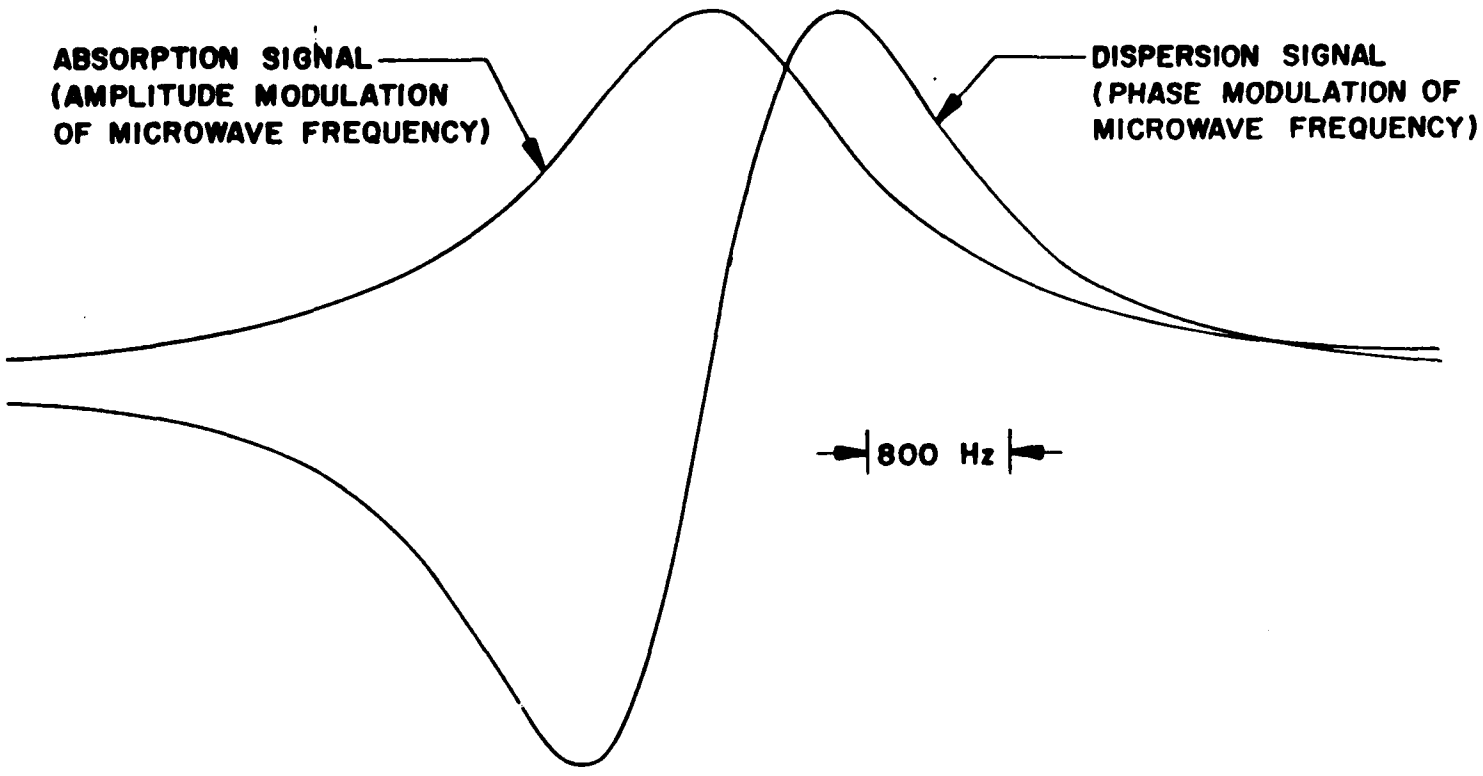

FIG.3-2

MAGNETIC RESONANCE SIGNALS

parameters which have been studied include temperature, microwave power, and light intensity. These measurements are discussed separately below. Linewidth measurements are made from the amplitude modulation signal, whereas frequency measurements are made from the phase modulation signal.

3.2 LINEWIDTH VS. TEMPERATURE

The magnetic resonance linewidth is not expected to be dependent on the resonance cell temperature, until temperatures greater than 150°C are reached. At lower temperatures the saturated Rb number density in the vapor is small enough that spin-exchange relaxation is not important. Since this is the major temperature dependent contribution to linewidth, no effects are expected at lower temperatures.

In fact, a very pronounced dependence of linewidth on temperature has been observed. This dependence has been thoroughly documented, and carefully studied. The measurements, as well as an explanation for the observations are described in the manuscript attached as Appendix A to this report.

The basic observation is that the linewidth decreases by about 40% as the temperature of the Rb cell is increased from 60°C to 90°C. This dramatic linewidth narrowing is explained as a non-linear effect due to absorption of light in the vapor. At higher temperatures more light is absorbed, and the linewidth becomes characteristic of a vapor excited by lower intensity radiation.

3.3 LINEWIDTH VS. LIGHT INTENSITY

A typical plot of linewidth vs. light intensity for a D_1 laser diode is shown in Figure 3-3. A direct extrapolation to zero light intensity yields a residual linewidth of 130 Hz FWHM. This residual linewidth is due to microwave power, relaxation, and inhomogeneous field broadening. It shows that these contributions to linewidth is actually very small.

A similar plot for a D_2 laser diode is shown in Figure 3-4. The extrapolated linewidth in this case is larger, reflecting the fact that the microwave power applied to the cavity is roughly 10 times larger.

3.4 LINEWIDTH VS. MICROWAVE POWER

A typical measurement of linewidth vs. microwave power is shown in Figure 3-5. The extrapolated value of 415 Hz is largely due to light intensity, which, using the relative scale of Figure 3-3, is 0.10.

3.5 FREQUENCY VS. LIGHT INTENSITY

The frequency dependence on light intensity is shown in Figure 3-6. A linear dependence is expected at these relatively low light levels and low temperatures. Absolute power levels corresponding to the relative intensity values given in the figure have not been

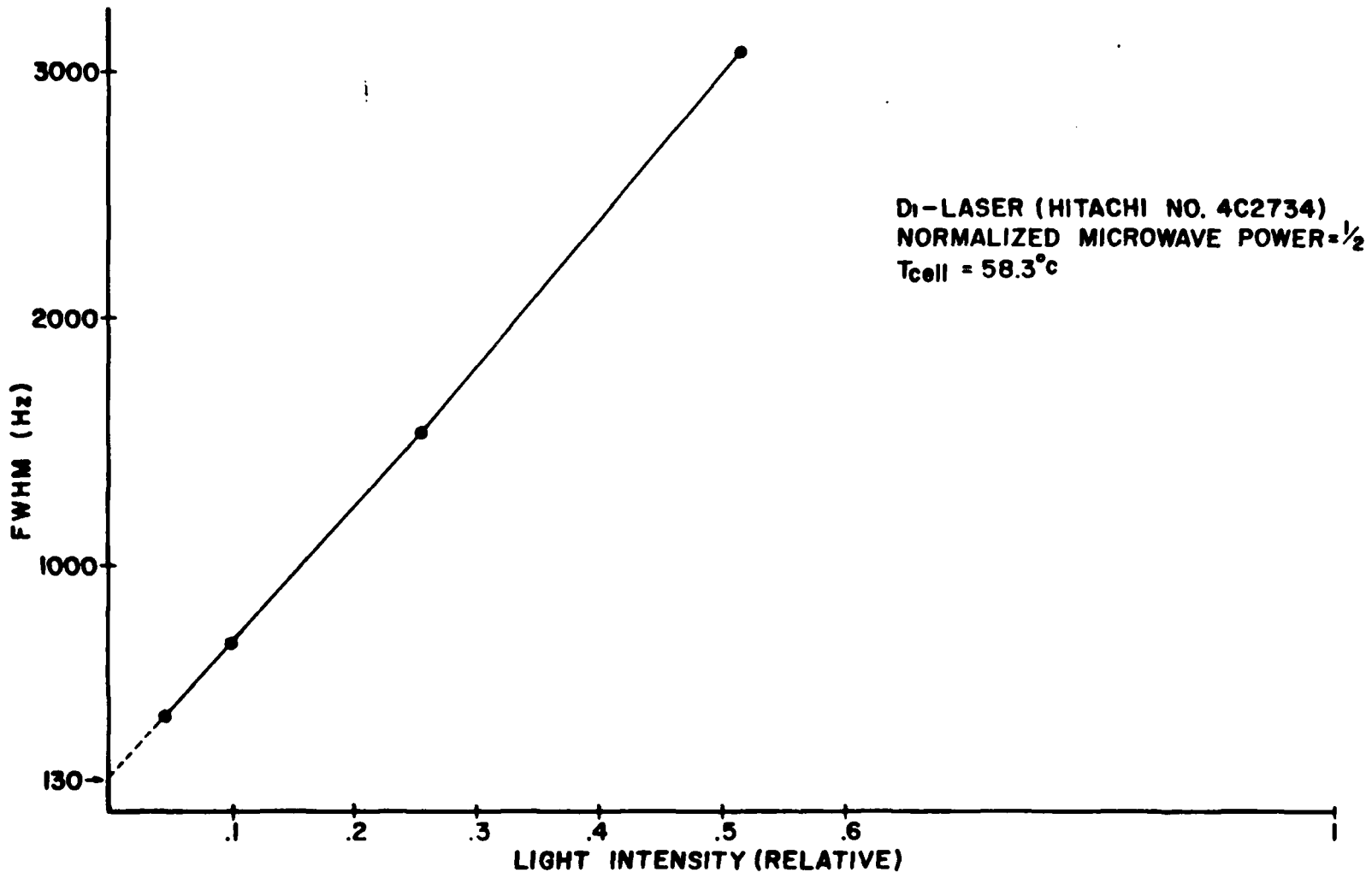

FIG.3-3

LINEWIDTH vs LIGHT INTENSITY (D1 LASER)

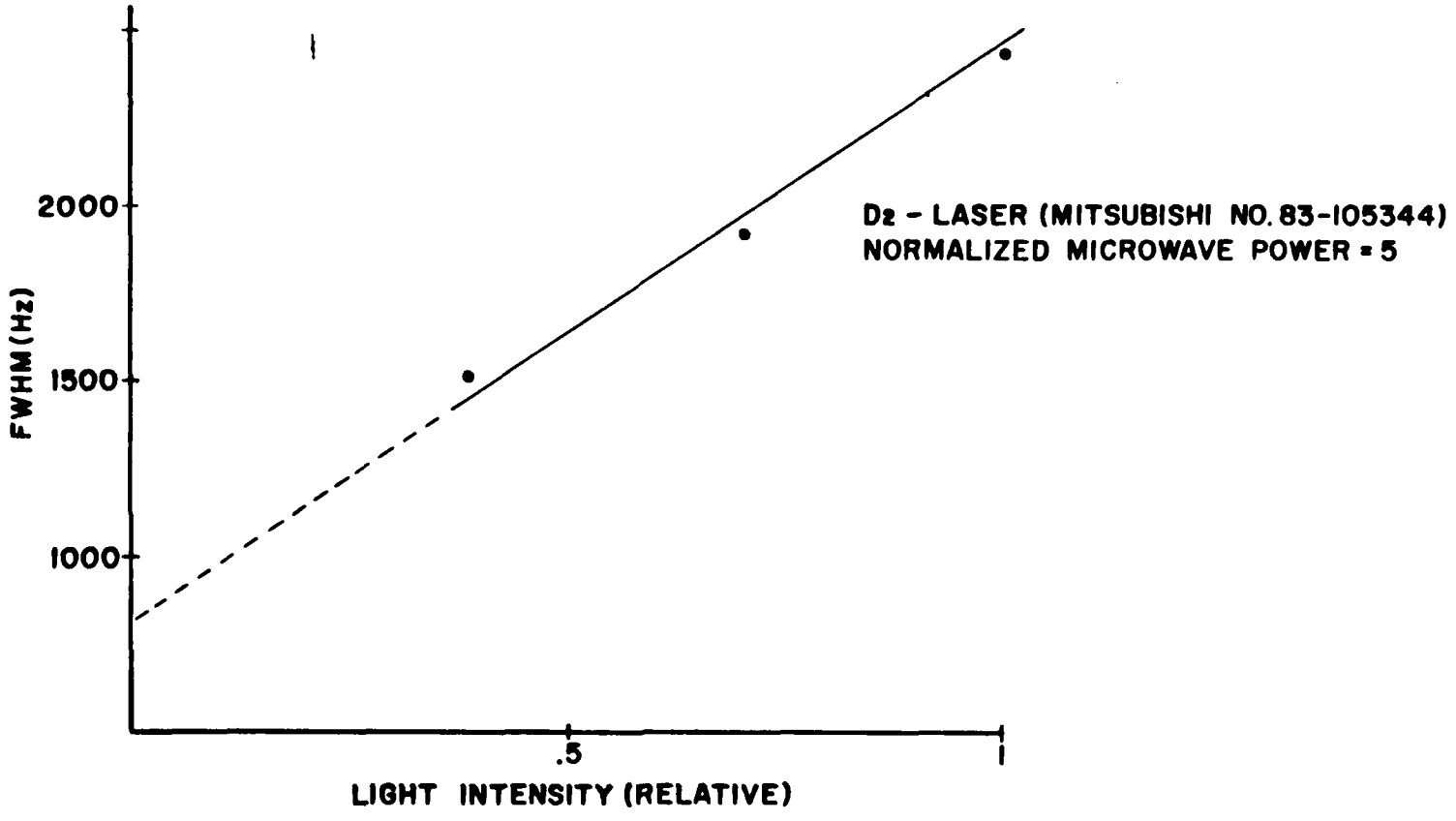

FIG.3-4

LINEWIDTH vs LIGHT INTENSITY (D_2 LASER)

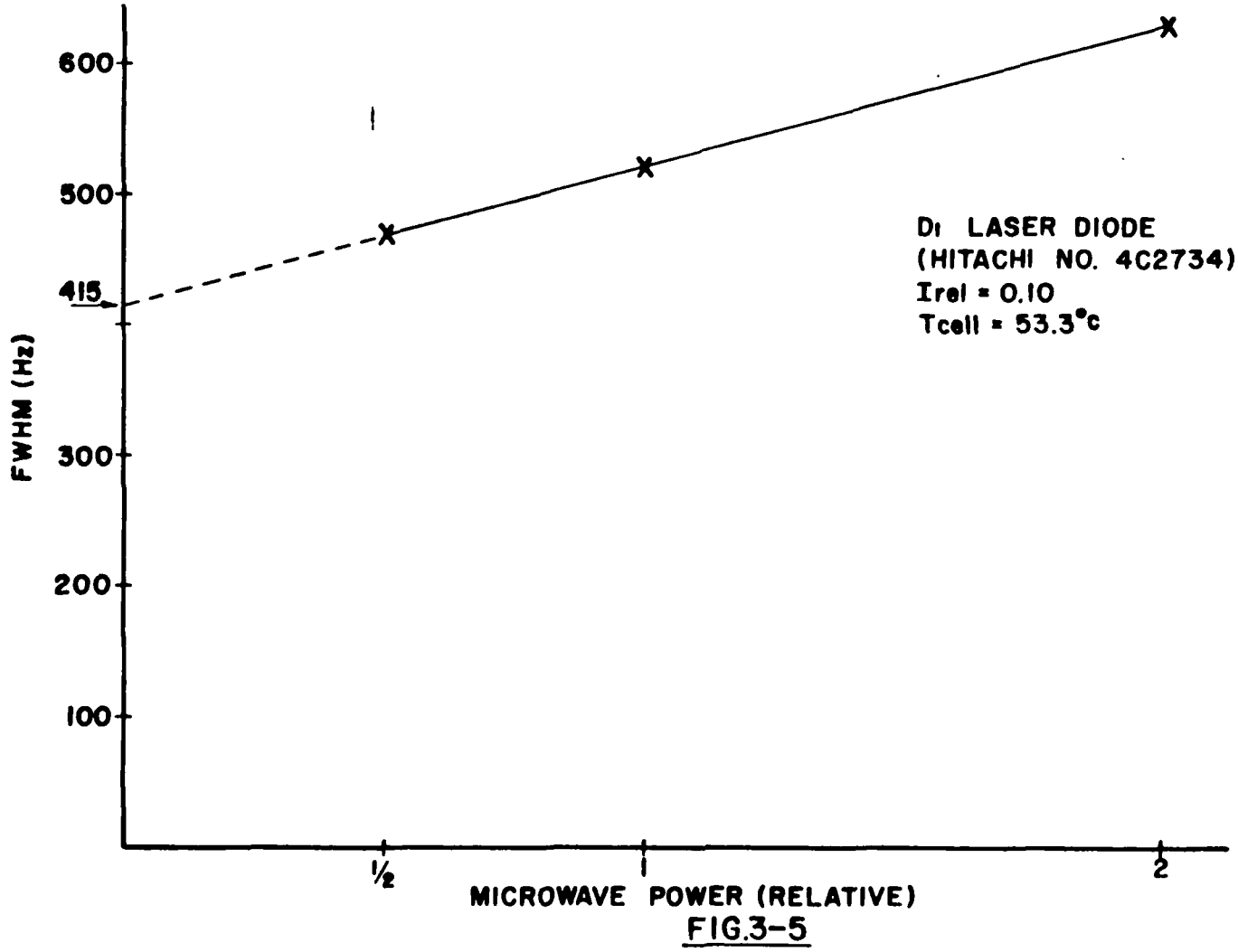

FIG.3-5

LINEWIDTH vs MICROWAVE POWER

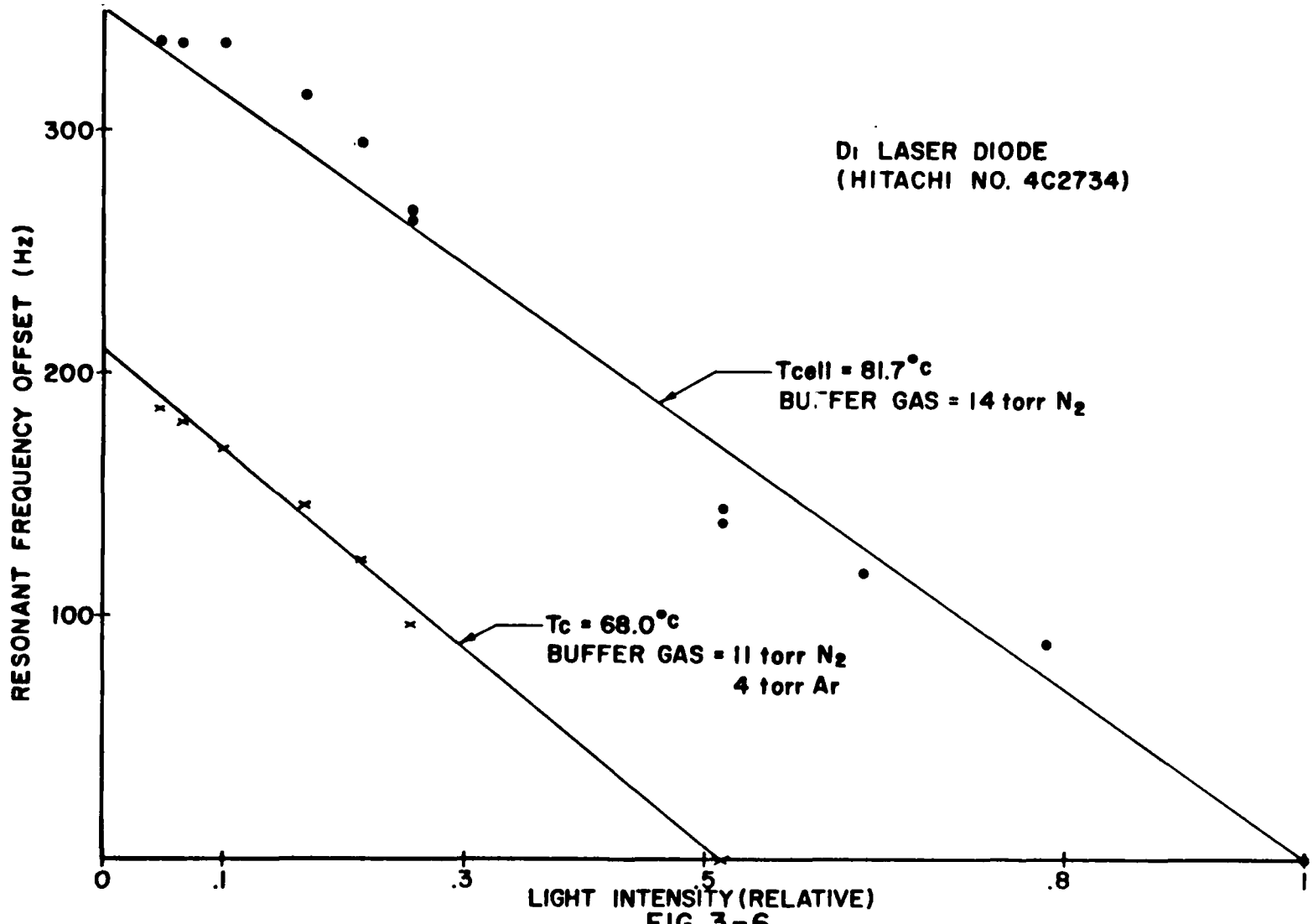

FIG. 3-6
RESONANCE FREQUENCY vs LIGHT INTENSITY

measured accurately, however, a rough correlation can be made. The relative values are normalized to the unattenuated laser output level which is measured to be ∿2.8 watts using the photodiode housed in the laser package. Because there are 8 uncoated glass surfaces between the laser and the Rb atoms we expect the actual unattenuated laser intensity to be ∿2.0 watts. The other values on the curve were obtained using neutral density filters placed in the light path.

3.6 FREQUENCY VS. MICROWAVE POWER

The relative microwave power input to the cavity can be measured using a pick-up loop near the cavity light opening. It has been found that variations of 14.5 dB in the power level measured this way have less than 1.5×10^{-10} (1 Hz at 6.834 GHz) effect on the frequency. This represents the entire microwave power dynamic range for the cavity drive circuitry.

This result indicates the absence of spurious microwave sidebands which can cause Bloch-Seigert type frequency shifts. The expected magnitude of such a shift is[2]

$$\Delta\omega_i = \frac{\beta_i^2}{2\hbar^2(\omega_o - \omega_i)} \qquad (3.1)$$

where β_i is the microwave power associated with the ith sideband, located at ω_i.

SECTION IV

CONCLUSIONS

4.1 CONCLUSIONS

We have studied both theoretically and experimentally the ground state hyperfine frequency shifts and line broadening mechanisms in Rb^{87}. Some of the observed effects are well understood, and some require further study.

The narrowing of magnetic resonance lines in optically thick vapors is predicted by theory. This effect is understood as a general effect independent of the specific geometry or cavity type. In fact this observation is even predicted for Zeeman optical pumping, in addition to hyperfine optical pumping. Understanding of this phenomenon is directly in line with the goals of this research, and very encouraging to the overall program.

Numerous other observations have been made of frequency and linewidth effects, as documented in Section II of this report. These observations have not yet been submitted to the careful scrutiny given the measurements associated with the narrowing effect. It is clear that such study is necessary in order to understand fully the physics associated with the hyperfine structure of Rb^{87}, and it is hoped that a continuation of this work can be carried out in the near future.

REFERENCES

1. T. McClelland and T. M. Kwon, AFOSR Annual Report, 1983 (Unpublished).

2. N. F. Ramsey, Phys. Rev. 100, 1191 (1955).

APPENDIX A

ANOMOLOUS NARROWING OF MAGNETIC RESONANCE LINEWIDTHS IN OPTICALLY PUMPED ALKALI METAL VAPORS

T. McClelland*, L. K. Lam, and T. M. Kwon

Litton Guidance and Control Systems, Inc.
5500 Canoga Avenue
Woodland Hills, CA 91365

*Present Address: Frequency Electronics, Inc.
55 Charles Lindbergh Blvd.
Mitchel Field, N.Y. 11553

ABSTRACT

Narrowing of Magnetic resonance lines in a dense optically pumped alkali metal vapor (Rb^{87}) has been observed. This observation is shown to be a result of optical pumping with a monochromatic light source tuned such that the real part of the vapor polarizability, which is responsible for light shifts, is essentially zero. A model based on the Bloch equations is used to describe the observed narrowing effect, and results of numerical calculations based on this model are presented. The results agree qualitatively with observations, and show correctly the disappearance of the effect at low light levels. This narrowing effect is of importance to the development of precision frequency standards and magnetometers utilizing monochromatic light sources (such as semiconductor lasers).

I. INTRODUCTION

Precision measurements of natural phenomena are often possible only because of the existence of narrow resonance lines. Naturally, effects which tend to broaden resonances degrade measurements, whereas those which tend to narrow resonances improve measurements. Motional narrowing[1], and Dicke narrowing[2] are well known examples of effects which enhance magnetic resonance measurements in atomic vapors. Precision atomic vapor frequency standards (which today routinely achieve stabilities of 10^{-11}/month) are possible because Dicke narrowed lines, orders of magnitude narrower than normal Doppler broadened lines, are achieved by atomic confinement to volumes $V \sim \lambda^3$ or smaller.

In this paper, we report a previously unobserved narrowing of magnetic resonance lines in optically pumped alkali metal vapors. We observe resonance linewidths to decrease with increasing temperature under conditions for which the lines would ordinarily be expected to be independent of temperature, or even to increase slightly with temperature. (Camparo et. al.[3] recently reported the observation of magnetic resonance lines inhomogeneously broadened due to light shift effects in optically pumped alkali metal vapors. Although their measurements were taken at a single temperature, one would expect the light shift effects they describe to produce a positive coefficient of linewidth with temperature rather than a negative coefficient, as we observe.)

For a temperature increase of 30°C, corresponding to roughly an eight-fold increase in atomic number density, we observe a linewidth narrowing of ~40%.

We observe the line narrowing effect under conditions of high light intensity, such that the total linewidth is dominated by the light contribution. (High light intensity here implies saturation of the ground state magnetic resonance transition, not saturation of the optical transition. The excited state decay rate is always much faster than the absorption rate in our experiments, so effects related to optical saturation can be ignored.)[4] The effect vanishes when the intensity is reduced sufficiently that other terms dominate the linewidth, suggesting that the narrowing is in fact produced by the light.

A contrasting explanation of our observations as a spin-exchange narrowing effect[5,6] proves inconsistent with the measurements. By extrapolating to zero light intensity and zero RF power we obtain an upperbound for relaxation contributions, including spin-exchange, to linewidth. We find the relaxation contribution to linewidth to be negligible under all conditions for which narrowing is observed.

We also find that the temperature range over which the narrowing is most dramatic corresponds to a transition within the vapor from "optically thin," at low temperatures, to "optically thick" at high temperatures. In these experiments temperature

determines the number of alkali atoms in the saturated vapor. The magnetic resonance is observed by monitoring the transmission of light through the vapor; and accordingly the effect is large over a range of temperatures such that at the low end the light transmission is large (>90%), and at the high end the transmission is small (<20%).

Finally, we observe the narrowing to occur for very narrow spectrum light tuned to the vapor absorption line center, where light shift effects are small. The availability of tunable single mode lasers is crucial to investigation of this regime.

In Section II we present a phenomenological model with which to explain the observed narrowing. We show that the effect is a natural result of optical pumping with a very narrow spectrum light source in the optically thin to thick transition temperature range, and is thus predicted for both Zeeman and hyperfine optical pumping experiments.

In Section III we discuss the hyperfine optical pumping experiment in which we have observed the line narrowing effect; and compare our measurements to numerical calculations based on the model described in Section II.

In Section IV we discuss some limitations of the model presented in Section II, and describe possible improvements. Practical applications are also briefly discussed.

II. TWO-LEVEL OPTICAL PUMPING MODEL

A. General Theory

We consider an ensemble of spin-1/2 atoms, with 2 ground state sublevels, excited by resonance electric dipole radiation, as in Figure 1. Such a system closely approximates alkali metal atoms in many optical pumping experiments.[7] In particular, it can be used to describe both Zeeman pumping with circularly polarized light, in which case the sublevels 1 and 2 represent Zeeman sublevels; or hyperfine pumping, in which case the sublevels 1 and 2 represent ground state hyperfine multiplets. Optical pumping results in a large population imbalance between ground state sublevels, and allows the ground state transition $E=\hbar\omega_o$ to be measured by magnetic resonance techniques.[1,8]

Theoretical description of the optical pumping process in optically thin vapors has been studied exhaustively by numerous workers;[7,8] however, optical pumping in thick vapors has received relatively little attention. In optically thin vapors, the non-linear differential equations describing the pumping process can be linearized, and solved in closed form, whereas in optically thick vapors the linear

approximations are no longer valid, and the equations must be solved numerically. With present computing capabilities such calculations can be carried out successfully for many systems, but the results tend to yield accurate predictions only for specific geometries, field configurations, buffer gas densities, etc.[3] They rarely give intuitive insight regarding the physics that didn't exist previously. In the following, we present simplified theoretical arguments based on the Bloch equations. We show that the results do not depend on specific geometries or field configurations, but are quite general in nature.

A schematic diagram of the atomic system is shown in Figure 2. The atoms are excited by resonant radiation from a collimated beam of photons which define the laboratory z-axis. The transmitted radiation is monitored with a photodetector. It is assumed that the mean free path of atoms in the vapor is much smaller than the mean absorption length of the incident photons, a good assumption for typical optical pumping experiments in which the atoms are confined by buffer gases. An oscillating magnetic field is applied in order to induce magnetic resonance transitions between the ground state sublevels. Its orientation in the laboratory is dependent on the specific type of experiment; however, it is always perpendicular to some effective DC magnetic field. For Zeeman optical pumping experiments the oscillating field is

perpendicular to an externally applied field which is typically along the z-axis. In hyperfine pumping, the oscillating field is perpendicular to the hyperfine interaction field of some subset of the atomic ensemble. For example, if the oscillating field is applied along the laboratory z-axis, then optical pumping of the $m_z = 0$ sublevels of the hyperfine multiplets is measured.[7,8]

The basic equation describing the transmission of light through the vapor is,

$$\frac{\partial}{\partial z} \mathcal{I}(\nu,z) = -n\sigma(\nu,I)\, \mathcal{I}(\nu,z), \qquad (1.)$$

where n = atomic number density,

σ = absorption cross section,

$\mathcal{I}(\nu,z)$ = light intensity per unit frequency

The absorption cross section is actually the expectation value of a quantum mechanical operator,

$$\sigma = \mathrm{tr}\{\rho\hat{\sigma}\}, \qquad (2.)$$

where ρ is the density operator for the ground state of the atomic system. The cross section σ thus depends on the state of the atomic ensemble, which in turn depends on the light intensity. In optical pumping experiments, the atomic

ensemble eventually reaches a steady state, and therefore Eq. (1) need not contain the time, t, explicitly.

We write the density operator explicitly as a two by two matrix,

$$\rho = \begin{bmatrix} \rho_{11} & \rho_{12} \\ \rho_{21} & \rho_{22} \end{bmatrix} . \qquad (3.)$$

The matrix elements ρ_{11}, ρ_{22} give the populations for the levels 1 and 2, respectively, and satisfy the normalization condition

$$\rho_{11} + \rho_{22} = 1. \qquad (4.)$$

The off diagonal elements ρ_{12}, ρ_{21}, are the coherences excited by the magnetic resonance field.

The Bloch equations for the two level system of interest can be written as:[7,8,9]

$$\dot{\rho} = -\tfrac{1}{2}\{\Gamma\ \rho + \rho\ \Gamma\} + \tfrac{1}{2}\langle\Gamma\rangle + \begin{bmatrix} \gamma_1(\tfrac{1}{2}-\rho_{11}) & -\gamma_2\rho_{12} \\ -\gamma_2\rho_{21} & \gamma_1(\tfrac{1}{2}-\rho_{22}) \end{bmatrix}$$

$$-i\omega_1 \cos\omega t \begin{bmatrix} \rho_{21}-\rho_{12} & -(\rho_{11}-\rho_{22}) \\ (\rho_{11}-\rho_{22}) & -(\rho_{21}-\rho_{12}) \end{bmatrix}$$

$$-i(\omega_o + \delta\omega)\begin{bmatrix} 0 & \rho_{12} \\ -\rho_{21} & 0 \end{bmatrix} \tag{5.}$$

The first and second terms on the RHS of Eq. (5.) are optical pumping terms; the first term in brackets giving the pumping due to depopulation of the ground state, and the second term giving the pumping due to repopulation of the ground state from the excited state. The diagonal optical pumping rate matrix is given by:

$$\Gamma = \begin{bmatrix} \Gamma_1 & 0 \\ 0 & \Gamma_2 \end{bmatrix} \tag{6.}$$

where

$$\Gamma_1 = \int_o^\infty \mathcal{I}(\nu)\ \sigma_1(\nu)d\nu,$$

$$\Gamma_2 = \int_o^\infty \mathcal{I}(\nu)\ \sigma_2(\nu)d\nu. \tag{7.}$$

σ_1 and σ_2 are optical absorption cross sections for the levels 1 and 2 respectively:

$$\sigma_1(\nu) \equiv \langle 1 \left|\hat{\sigma}\right| 1\rangle,\ \sigma_2(\nu) \equiv \langle 2\left|\hat{\sigma}\right| 2\rangle.$$

Optical pumping occurs when $\Gamma_1 \neq \Gamma_2$. In Zeeman optical pumping with σ_+ light, Γ_1 is made to vanish because $\sigma_1(\nu) = 0$. For hyperfine pumping either Γ_1 or Γ_2 is made negligible by choosing filtered light such that one of the overlap integrals in Eq. (7) vanishes, while the other remains finite.

The third term on the RHS of Eq. (5.) is a phenomenological relaxation term, with

$\gamma_1 = \frac{1}{T_1}$ = longitudinal relaxation rate, and

$\gamma_2 = \frac{1}{T_2}$ = transverse relaxation rate.

The fourth term in Eq. (5.) is the magnetic resonance term, with ω the applied RF frequency, and ω_1 the Rabi frequency.

The last term in Eq. (5.) gives the dependence on static fields, $\hbar\omega_o$ being the energy separation due to these fields. For Zeeman pumping, $\omega_o = g_J\mu_B H_o$ and H_o represents an externally applied static magnetic field along the light propagation direction. For hyperfine pumping, $\hbar\omega_o$ represents the hyperfine interaction energy. The quantity $\delta\omega$ represents a shift of the frequency ω_o due to the light. This light shift, which is actually a manifestation of the AC Stark effect, has been studied in detail by Mathur, et. al.[10] They have shown that

$$\delta\omega = 2\pi \int_0^\infty \mathcal{I}(\nu)\mathcal{S}_{12}(\nu)\, d\nu, \qquad (8.)$$

Where $\mathcal{S}_{12}(\nu)$ is a light shift profile function. Although $\mathcal{S}(\nu)$ changes rapidly with frequency near resonance, peak values are typically $\sim$1-10 Hz/(μW/cm^2) for rubidium; both for Zeeman pumping and hyperfine pumping.

The relevant solutions of Eq. (5.) are well known.[8,9] One first solves Eqs. (5) for the coherence, ρ_{12}:

$$\dot{\rho}_{12} = -(\gamma_2 + \Gamma_{av} + i\omega_o)\,\rho_{12} + (i\,\omega_1 \cos\omega t)\,S, \qquad (9.)$$

Where we have made the substitutions

$$S \equiv \rho_{11} - \rho_{22} \qquad (10.)$$

and $$\Gamma_{av} \equiv \frac{\Gamma_1 + \Gamma_2}{2}\,. \qquad (11.)$$

Then one uses the secular approximation, in which the time dependence of ρ_{12} is assumed to be given by

$$\rho_{12} = \rho_{21}^* = \rho_o e^{-i\omega t}, \qquad (12.)$$

the time scale for ρ_o being much slower than the oscillations at frequency ω. It is found, keeping only slowly varying terms, that

$$\rho_o = \left\{ \frac{i\omega_1}{2} \Big/ \left[(\gamma_2 + \Gamma_{av} + i(\omega_o + \delta\omega - \omega) \right] \right\} S, \qquad (13.)$$

which upon substitution yields

$$\dot{S} = -\gamma_1 S - \Gamma_1 \rho_{11} + \Gamma_2 \rho_{22} - \frac{\omega_1^2 (\gamma_2 + \Gamma_{av})}{(\gamma_2 + \Gamma_{av})^2 + (\omega_o + \delta\omega - \omega)^2} S \qquad (14.)$$

Eq. (14) is easily solved for the steady state solution, $(\dot{S}=0)$,

$$S = -\frac{1}{2}(\Gamma_1 - \Gamma_2)\, \tau_1 \left\{ 1 - \frac{\omega_1^2 \tau_1 \tau_2}{1 + \omega_1^2 \tau_1 \tau_2 + \Delta\omega^2 \tau_2^2} \right\}, \qquad (15.)$$

where

$$\frac{1}{\tau_1} \equiv \Gamma_{av} + \gamma_1$$

$$\frac{1}{\tau_2} \equiv \Gamma_{av} + \gamma_2$$

$$\Delta\omega \equiv (\omega_o + \delta\omega) - \omega$$

Eq. (15.) together with Eq. (4.) gives the desired solution for the ground state populations, ρ_{11}, ρ_{22} as a function of z.

Eq. (1.) can now be written as

$$\frac{\partial}{\partial z}\ \mathcal{I}(\nu,z) = -\,n\,\mathcal{I}(\nu,z)\left\{\sigma_1(\nu)\frac{(1+S)}{2} + \sigma_2(\nu)\frac{(1-S)}{2}\right\}. \quad (16.)$$

Of course, in any experiment it is not $\mathcal{I}(\nu,z)$ which is measured, but

$$\int_a^b d\nu \mathcal{I}(\nu,z).$$

Typically, we can take the integration range as 0 to ∞ without loss of generality. When Eq. (16.) is integrated in this fashion, we obtain

$$\frac{\partial I}{\partial z} = -\,n\left\{\Gamma_1\,\frac{(1+S)}{2} + \Gamma_2\,\frac{(1-S)}{2}\right\} \quad (17.)$$

$$= -\,n\,\frac{(\Gamma_1+\Gamma_2)}{2} - n\,\frac{(\Gamma_1-\Gamma_2)}{2}\,S,$$

where we have substituted

$$I(z) \equiv \int_0^\infty d\nu \mathcal{I}(\nu,z).$$

We are interested in solutions of Eq. (17.), given a specified incident light intensity,

$$I_o \equiv I(z=o) = \int_0^\infty d\nu\ \mathcal{I}_o(\nu,z=o),$$

and clearly these solutions depend critically on the incident light spectrum. However, in optical pumping experiments, the incident light is prepared such that either Γ_1, or Γ_2 tends to vanish. In what follows, we assume that only one of the Γ's is non-zero; this assumption is rigorously met in

single mode laser optical pumping experiments (such as the one described in Section III), but is a slight simplification of experiments using resonance light of broad spectral profile. Even in these cases, however, it gives a good qualitative description of the optical pumping process.

With this assumption it is easy to show that Eq. (17.) simplifies to

$$\frac{\partial I}{\partial z} = -n \frac{\Gamma_\alpha}{2} (1+\tilde{S}), \quad \text{where} \tag{18.}$$

$$\tilde{S} = -\frac{1}{2} \Gamma_\alpha \tilde{\tau}_1 \left\{ 1 - \frac{\omega_1^2 \tilde{\tau}_1 \tilde{\tau}_2}{1 + \omega_1^2 \tilde{\tau}_1 \tilde{\tau}_2 + \Delta\omega^2 \tilde{\tau}_2^2} \right\} \text{ and}$$

$$\frac{1}{\tilde{\tau}_1} = \frac{\Gamma_\alpha}{2} + \gamma_1,$$

$$\frac{1}{\tilde{\tau}_2} = \frac{\Gamma_\alpha}{2} + \gamma_2, \text{ for } \alpha = 1 \text{ or } 2.$$

Eq. (18.) must still be solved numerically, but can easily be handled by computer.

It is useful to examine Eq. (18) in the absence of an oscillating magnetic field, i.e. $\omega_1=0$. We write for later reference the asymptotic limits of Eq. (18.) for high and low light intensity.

$$\frac{\partial I}{\partial z} = -n \gamma_1 \left[1 - \frac{2\gamma_1}{\Gamma_\alpha} \right] \quad ; \frac{\Gamma_\alpha}{2\gamma_1} >> 1 \tag{19a}$$

$$\frac{\partial I}{\partial z} = -\frac{n\Gamma_\alpha}{2} \left[1 - \frac{\Gamma_\alpha}{2\gamma_1} \right] \quad ; \frac{\Gamma_\alpha}{2\gamma_1} << 1. \tag{19b}$$

At high light levels the intensity falls off linearly with path length through the vapor; whereas at low light levels the transmission reduces to the familiar exponential decay, which is valid whenever optical pumping effects are absent.

B. High Light Levels

To understand the experimentally observed narrowing phenomena, we present a heuristic argument. Consider the situation when the optical pumping rate, Γ_α, is large compared to all other relaxation terms:

$$\Gamma_\alpha >> \frac{1}{\tau_1} , \frac{1}{\tau_2} , \omega_1 ;$$

and the light shift, $\delta\omega$, is zero. These are reasonable approximations for the experiment described in Section III, in which Rb^{87} atoms are optically pumped with a semiconductor laser. The polarizability of Rb^{87} vapor in the vicinity of a D_1 absorption resonance is shown in Figure 3. By tuning a narrow, single mode laser to the peak of the absorption curve (α''), the light shift (α') becomes zero. It is then easy to show that Eq. (18.) reduces to

$$\frac{\partial I}{\partial z} = \frac{-n\Gamma_\alpha}{2} \left\{ 1 - \left[1 - \frac{\omega_1^2}{(\Gamma_\alpha/2)^2 + \Delta\omega^2} \right] \right\} \qquad (19.)$$

$$= - \frac{n\Gamma_\alpha}{2} \left\{ \frac{\omega_1^2}{(\Gamma_\alpha/2)^2 + \Delta\omega^2} \right\} ,$$

where we have assumed for simplicity that $\gamma_1 = \gamma_2$. If the vapor is optically thin, such that

$$\frac{1}{n\sigma_\alpha} >> \ell,$$

where ℓ is the total optical path length, then Eq. (19.) is easily integrated yielding

$$I(z=\ell) = I_o - \frac{n\Gamma_{\alpha o}\ell}{2}\left\{\frac{\omega_1^2}{\frac{\Gamma_{\alpha o}}{2}^2 + \Delta\omega^2}\right\}, \qquad (20.)$$

where

$$\Gamma_{\alpha o} = \int_o^\infty \mathcal{I}_o(\nu)\sigma_\alpha(\nu)d\nu.$$

Eq. (20.) shows that for the given assumptions, the transmitted intensity vs. RF frequency, ω, is a Lorentzian function, with

$$\text{FWHM} = \Gamma_{\alpha o}\text{, and} \qquad (21.)$$

$$\text{amplitude} = \frac{(\omega_1^2\ n\ \ell)}{(\Gamma_\alpha/2)}. \qquad (22.)$$

The area under the Lorentzian is conserved, and therefore, as the incident light intensity is increased, the resonance is broadened, but with commensurate loss of amplitude.

The transmission of an optically thick vapor can be obtained iteratively from Eq. (20.); the total path length of the light is divided into segments, ℓ, each small enough that Eq. (20.) is valid over the length of the segment. Then

$$I_{N+1} \quad I(z=(N+1)\,\ell) = I_N - n\Gamma_{\alpha N}\ell\left[\frac{\omega_1^2}{\left(\frac{\Gamma_{\alpha N}}{2}\right)^2 + \Delta\omega^2}\right]. \qquad (23.)$$

The important feature is that since

$$\Gamma_{\alpha(N+1)} < \Gamma_{\alpha N}$$

for all N, the Lorentzian resonances contributed by successive segments become larger in amplitude and narrower in width. We anticipate, on the basis of Eq. (23.) that optically thick vapors should produce narrower transmission resonances than optically thin vapors.

If the light shift, $\delta\omega$, is non-zero, this reasoning must be altered slightly. We still expect the above arguments to hold for the light shifted resonances, except that resonances contributed by successive segments are shifted less and less due to the fact that the light shift is proportional to intensity. Because the light shift can easily be several times as large as the resonance width in optical pumping experiments,[10] the observed transmission resonance in an optically thick vapor tends to be broadened rather than narrowed. One can think of the observed resonance as an envelope formed from discrete light-shifted resonances in in each segment. Thus even though the resonance linewidths in successive segments tend to become narrower, the envelope formed of all segments has a characteristic (inhomogeneous)

width given by the difference between the light shift at the entrance window, and the exit window of the vapor.

This inhomogeneous broadening was observed for hyperfine optical pumping by Camparo, et. al.[3] Its light shift origin was demonstrated by comparing the transmission resonance lines obtained with an optical source tuned to yield a positive light shift to that obtained with a source tuned to yield a negative light shift. In both cases the resonance line had a peak near the unshifted line center; however a positive light-shift source produced a broad shoulder on the positive frequency side of ω_o, whereas a negative light shift source produced a broad shoulder on the negative frequency side of ω_o. This is exactly the prediction of Eq. (23).

In summary, we explain the observation that resonance lines can be broader in optically thick vapors than in optically thin vapors as a light shift phenomenon. However, we expect that resonances observed in vapors excited with zero-lightshift producing radiation should get narrower as optical thickness is increased. Of course we also expect that for low light levels, such that the linewidth is dominated by other influences, the resonances should be independent of optical thickness.

III. EXPERIMENT

A. Experimental Set-Up

We have observed this line narrowing effect in hyperfine optical pumping studies, in which Rb^{87} is optically pumped by a single-mode semiconductor laser light source, tuned to the Rb D_1 resonance. The experimental set-up is shown in Figure 4.

The light source is a commercially available Hitachi laser diode (Model No. 7801). Its output is a function of both junction temperature and forward bias current. Junction temperature is controlled by mounting the diode on a heat-sink, which in turn is temperature-stabilized by a thermoelectric oven to ±0.1°C. Forward bias current is provided by a stable (±0.001mA) constant current supply. The resulting laser output spectrum, as measured on a Fabry Perot spectrum analyzer, is shown in Figure 5. Total laser intensity is ∿3mW.

The laser output is collimated and then transmitted through a cylindrical resonance cell (1 cm. i.d., 1cm long) containing isotopically pure Rb^{87}, and buffer gases. Typically, the cell contains 10-15 torr of Argon and/or 10 torr of N_2 (measured at room temperature). These buffer gases slow

diffusion of Rb atoms, effectively confining them to a region small compared to the vapor length (in agreement with the assumptions of Section II); in addition N_2 quenches the Rb excited state emission and thereby enhances the optical pumping.[7]

The resonance cell is located inside a microwave cavity tuned to the 6.834 GHz. hyperfine resonance frequency of Rb^{87}. (This is the magnetic field insensitive m=0→m=0 transition.) The cavity is of rectangular cross-section and operates in the TE_{101} mode. In order to enhance the uniformity of the microwave field, and also to reduce size, the cavity is partially loaded with a glass-ceramic dielectric material (Corning Macor). Performance of this cavity has been described in a previous paper.[11]

Resonance cell temperature is controlled by bi-filar resistive heater foils glued onto the outside surface of the cavity. The temperature is monitored by a platinum resistive sensor on the cavity, which is also used to servo-control the temperature. A temperature stability of ±0.2°C is obtained over typical measurement periods. The entire cavity assembly is positioned inside a pair of DC magnetic field coils, which produce a static field of ∿300 mG along the optical transmission axis.

Laser light transmitted through the resonance cell is monitored with a silicon photodiode. It contains two AC signal components; one at approximately 6 kHz which results from modulation of the laser diode bias current, and one at approximately 40 Hz which results from amplitude modulation of the microwave field.

The signal at 6 kHz is fed back to the laser diode current control, in order to lock the laser diode output to the Rb^{87} absorption line center. This active stabilization of the laser optical frequency nominally reduces the light shift to zero since the absorption line center frequency is also the zero crossing of the light shift profile function, $\mathcal{S}_{12}(\nu)$. In addition, light shift fluctuations due to frequency instability of the laser are minimized.

Such noise fluctuations have been measured by locking a Voltage Controlled Crystal Oscillator (VCXO) to the Rb hyperfine frequency in place of the cesium reference (Figure 4), and measuring the Allan Variance of the VCXO output.[12] The Allan Variance was measured using a modified version of the dual mixer time difference system developed by NBS, with a commercial cesium frequency standard (FTS model No. 4050) as the reference.[13] The results are shown in Figure 6, for

laser output attenuated by a factor of 10. Using $\sigma_y^2(\tau)$ as a measure of fractional frequency fluctuations,[12] where f_o = 6.834 GHz, we calculate the total noise contribution to resonance linewidth to be $\gtrsim$1 Hz. Even if all the measured noise were due to light shift fluctuations (which are proportional to intensity), the total linewidth contribution for an unattenuated laser would be $\gtrsim$10 Hz; an amount much smaller than the measured narrowing effect.

The AC photocurrent at 40 Hz gives the magnetic resonance signal. The frequency synthesizer output is amplitude modulated at this frequency, and then swept slowly through the resonance region, at $\sim$80 Hz/sec. A typical hyperfine resonance line measurement is shown in Figure 7.

II. RESULTS

Figure 7 shows two measured resonance lines; one at low temperature and one at high temperature. It is clear from the figure that the linewidth is dramatically decreased at the higher temperature. Both curves are measured using the same incident light intensity ($\sim$1mW). The "dark" width of the lines, measured by extrapolating to zero light intensity, is $\sim$210 Hz, so that most of the observed linewidth is due to light.

Figure 8 shows for comparison the predicted results based on numerical integration of Eq. (18.). For these numerical calculations the laser spectrum is treated as a delta function tuned to the peak of the absorption profile and the zero crossing of the light-shift profile of the vapor. (See Figure 3.)

Figure 9 is a plot of linewidth vs. temperature. the experimental data was obtained when incident light intensity was made to dominate the total linewidth. It is clear from the data that whereas both experiment and theory show a definite narrowing of linewidth with temperature, the measured narrowing is considerably larger than the theoretical narrowing predicted by the simplified model of Section II. The error bars on the experimental data represent linewidth uncertainties associated with a single curve; they are thus related to the signal to noise ratio of each measurement, but do not represent a statistical spread of data.

Figure 10 shows linewidth vs. temperature data for the contrasting conditions of high and low light intensity; we see from the figure that the narrowing effect is present with high light intensity, but absent with low light intensity. The results of numerical computation for low light intensity are also shown in this figure, and, as expected predict no dependence of linewidth on temperature.

Every effort has been made to eliminate the possibility of systematic errors in measurement of the narrowing effect. Because the microwave cavity serves also as oven for the resonance cell, it might be supposed that the effect is actually due to changing effective microwave power densities at the cell due to thermal changes in the cavity walls. This is ruled out, however, since all measurements are made under conditions in which the total microwave power contribution to linewidth is much smaller than the measured temperature effect. (See Figure 9.) Furthermore, actual measurements of microwave power with a pick-up loop near the cell indicate that the power changes no more than 2 dB over the temperature range 60-86°C. Finally, the disappearance of the effect at low light levels, for identical microwave power settings, argues against this supposition.

Similarly, we rule out thermal effects in the DC magnetic field coils as a cause of the effect. The inhomogeneous field contribution to linewidth must be less than the residual, non-light induced linewidth, which is measured to be ∿130 Hz at 60°C for very low microwave power output. The resonance measured is the 0-0 hyperfine transition which is insensitive in first order to magnetic field. In order to account for the observed narrowing effect in this way it would be necessary for the 30°C temperature span to introduce a field inhomogeneity roughly 4 times the

nominal value of the field at 60°C. This is completely implausible, since any change in inhomogeneity must be due to changes in shape and/or aspect ratio of the C-field coil forms. Huge thermal gradients across the solid aluminum cavity/coil form structure would be necessary to generate such changes.

Another systematic linewidth effect is possible from the laser modulation current at 6 kHz. This modulation causes the light shift to oscillate at 6 kHz, contributing to the linewidth an amount equal to the peak to peak light shift excursion. The level of modulation must be kept small enough that this linewidth contribution is negligible, as it would be expected to decrease with vapor density just as the observed effect does. In our experiments the measured modulation contributes $\sim$200 Hz/mW to the linewidth; much less than the observed effect. In addition, a check has been made by scanning the lines with the modulation current removed (6 kHz feedback loop open). In this case the linewidth still decreases with temperature, just as in the locked case.

IV. DISCUSSION

Our measurements show a very substantial narrowing of microwave magnetic resonance linewidths with increasing temperature, an effect which we interpret as due to attenuation of the optical pumping rate by an increasingly dense vapor. The numerical results based on the phenomenological model of Section II agree qualitatively with our experimental observations, predicting well the narrowing of linewidth with temperature for high incident light intensity; as well as the disappearance of any temperature dependence at low incident light intensity. However, the quantitative agreement between the model and experiment is not as good, since we observe a $\sim$40% effect and the numerical results predict a $\sim$10% effect. This is perhaps not too surprising given the limitations of the model.

The model treats the ground state as a two level system, whereas the Rb^{87} ground state actually has 8 sublevels. It is an oversimplification to consider atoms in the two sublevels connected by the magnetic resonance transition as a closed system, since the populations of these sublevels are affected by the other 6 sublevels. For example, the incident light produces a nonlinear birefringent polarizability in the vapor (unless the light is completely isotropic) which results in alignment of the ground

state sublevel populations.[10] This birefringence changes the effective pumping rate, Γ, and alignment changes the relative sublevel populations; both of which affect the optical pumping signal.

A more accurate model would replace the simple two by two density matrix of Eq. (3.) by an n x n matrix describing the appropriate atoms. We have begun calculations based on such a model.[15] In these calculations we solve the density matrix rate equation in the spherical tensor basis, thus taking advantage of the spherical symmetry of the problem and accounting for all the non-isotropic interactions between the radiation and the atoms.[16]

The predictions of our simple model are also limited by the fact that they ignore any dependence of the fields on the transverse coordinates. In particular, focusing/defocussing of the light is ignored, which is certainly a good first order approximation of the collimated beam from a laser diode, but never exactly true. We measured the divergence of the beam to be less than $\pm 1^\circ$ from the optic axis in the horizontal plane, but because of a small astigmatism, we expect the divergence in the vertical plane to be slightly greater. (The divergence in this plane could not be accurately measured because of limitations in our apparatus.) It must be noted, however, that even a 1°

divergence produces a 7% change in light flux over the length of a 1 cm long cylindrical cell 1 cm in diameter; independent of the atomic vapor inside the cell.

A diverging beam would be expected to amplify the predicted narrowing effect by the following argument. The decreasing light intensity with path length through the cell (due to divergence) makes the vapor appear hotter than it really is. We see from Figure (9) that the slope of the theoretical linewidth vs. temperature curve increases with increasing temperature. Thus we expect the measured curve to exhibit an increased slope, corresponding to higher temperatures.

Qualitatively, we can understand this by examining Eqs. (19.) and noting that the relative absorption,

$$\frac{1}{I}\ \frac{\partial I}{\partial z}\ ,$$

in an optically pumped vapor always varies inversely with light intensity; only approaching asymptotically at low light levels the constant value characteristic of absorption in a vapor with no optical pumping. Hence, any external mechanism which attenuates the light also increases the absorption, making the vapor appear more dense.

The narrowing effect as explained herein is seen to be an outcome of optical pumping in dense vapors with very intense resonant radiation. As such it might be viewed as of questionable practical interest, since only highly light-broadened lines are narrowed, a result which seemingly is better achieved by operating at lower light intensity in less dense vapors. For spectroscopic applications this is perhaps true, but for practical devices based on atomic vapor magnetic resonance, such as magnetometers and frequency standards, this is not true. The increased number of atoms in a dense vapor can be effectively sampled only with intense optical pumping radiation, and larger signal to noise ratios are achievable. It is well known, for instance, that the short term stability of an atomic vapor frequency standard is generally worse than that of a good crystal oscillator because of the small number of atoms sampled in an atomic vapor (typically 10^{12}) compared to a crystal ($>10^{20}$).[17] Presently available atomic frequency standards are only beneficial for long measurement times, such that the fluctuations associated with the atomic vapor are averaged out. By using an intense monochromatic light source carefully tuned to eliminate light shifts, it is possible to improve performance in such devices, not only because of the increased optical pumping efficiency, but by significantly narrowing the magnetic resonance lines.

ACKNOWLEDGEMENTS

We wish to thank J.C. Camparo of the Aerospace Corporation for helpful discussions regarding the observed line narrowing. In addition, we are grateful to M. Bloch and Frequency Electronics, Inc. for granting the time and facilities needed to prepare this manuscript.

This work has been sponsored by the Air Force Office of Scientific Research, under Contract No. F49620-83-C-0132.

REFERENCES

1. C. P. Slichter, Principles of Magnetic Resonance, Springer-Verlag (1980).

2. R. H. Dicke, Phys. Rev. 89, 472 (1953).

3. J. C. Camparo, R. P. Frueholtz, and C. H. Volk, Phys. Rev. A 27, 1914 (1983).

4. C. Cohen-Tannoudji, Metrologia 13, 161 (1977).

5. W. Happer, and A. C. Tam, Phys. Rev. A 16, 1877 (1977).

6. J. C. Camparo, and R. P. Frueholtz, Phys. Rev. A 31, 1440 (1985).

7. W. Happer, Rev. Mod. Phys. 44, 169 (1972).

8. L. C. Balling, Advances in Quan. Elec. 3, 1 (1975).

9. G. Missout, and J. Vanier, Can. J. Phys. 53, 1030 (1975).

10. B. S. Mathur, H. Tang, and W. Happer, Phys. Rev. 171, 11 (1968).

11. H. E. Williams, T. M. Kwon, and T. McClelland, Proceedings 37th Ann. Freq. Control Symp. (1983).

12. J. A. Barnes, et al., IEEE Trans. on Instr. and Meas. IM-20, 105, (1971).

13. D. W. Allan, National Bureau of Standards, NBSIR 75-827. (1976).

14. B. S. Mathur, H. Tang, and W. Happer, Phys. Rev. A 2, 648 (1970).

15. T. McClelland, and T. M. Kwon, AFOSR Annual Report, 1983 (Unpublished).

16. Several authors have treated hyperfine optical pumping in real alkali metal vapors, but without accounting for non-isotropic interactions between the radiation and the atomic system. See refs. 3, 9.

17. L. S. Cutler, and C. L. Searle, Proc. IEEE 54, 136 (1966).

FIGURE CAPTIONS

FIGURE 1 — Energy level diagram for alkali metal atoms. The levels 1 and 2 can be either Zeeman sublevels or hyperfine levels.

FIGURE 2 — Schematic diagram of the atomic system upon which the model of Section II is based. Collimated resonance radiation which is transmitted through the interaction region is monitored by a photodetector.

FIGURE 3 — Hyperfine polarizability of Rb^{87} in the vicinity of the $F = 1 \rightarrow F = 1,2$ absorption line for D_1 light. The peak of the imaginary part of the polarizability (absorption) coincides with the zero-crossing of the real part of the polarizability (light shift). The widths of the resonances are typical of optical pumping experiments with $\sim$10 torr of buffer gas. These curves are calculated from expressions in Ref. 14.

FIGURE CAPTIONS

(continued)

FIGURE 4 — Schematic diagram of the experimental apparatus described in Section III.

FIGURE 5 — Spectral output of the laser diode, as measured with a confocal Fabry-Perot spectrum analyzer.

FIGURE 6 — Allan Variance as a function of averaging time for the experimental apparatus operated as a frequency standard. The solid line through the data gives the theoretically predicted slope for a frequency standard limited by shot noise.

FIGURE CAPTIONS

(continued)

FIGURE 7 — Typical measured magnetic resonance lines at two different temperatures. The residual width of the lines due to non-light causes was measured by extrapolation to zero light intensity, in a separate experiment. Assuming this residual width to be caused by a phenomenological relaxation, γ, and microwave field strength, ω_1, acting in quadrature, we can put an upper bound on its value of $2(\omega_1^2 + \gamma^2)^{1/2} < 210$ Hz.

FIGURE 8 — Typical theoretical magnetic resonance lines at two different temperatures. These curves are obtained by numerical integration of Eq. (18), assuming a delta function light source, and zero light shift. The values used for the relaxation rates, γ_1, and γ_2, and microwave field strength, ω_1, are shown.

FIGURE CAPTIONS

(continued)

FIGURE 9 — Magnetic resonance linewidth vs. temperature. The top curve gives the dependence predicted from numerical integration of Eq. (18). The bottom 2 curves give the measured dependence for two separate experiments, differing slightly by the amount of microwave power used to excite the resonance. An upperbound on the extrapolated residual linewidth is given in each case.

FIGURE 10 — Linewidth vs. temperature for high and low incident light intensity. Top curve shows the dependence for high light intensity, normalized to 1. Middle curve shows a similar measurement, but with I=0.09. In each case an extrapolated upper bound on the residual linewidth is given. The bottom curve shows the predicted dependence from numerical integraton of Eq. (18), for very low light intensity.

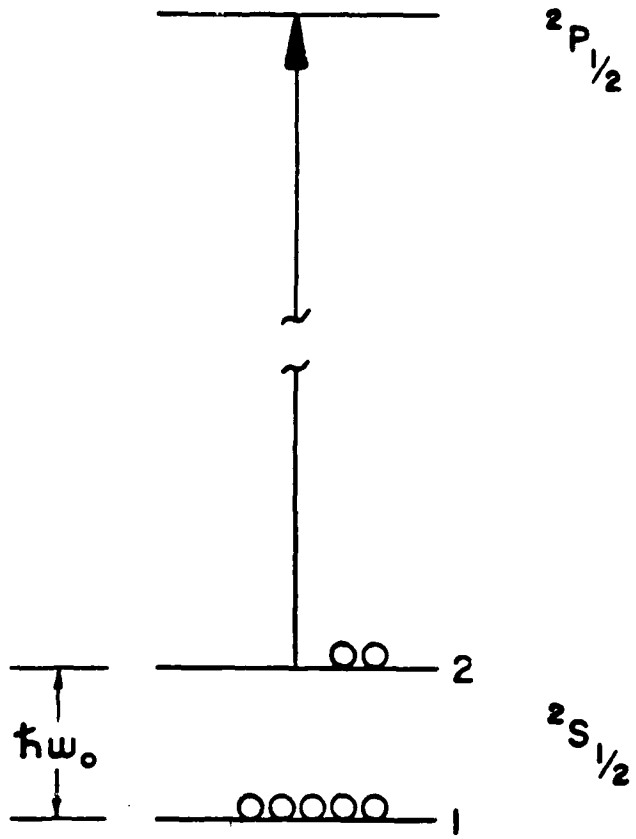

FIG. 1

ENERGY LEVEL DIAGRAM

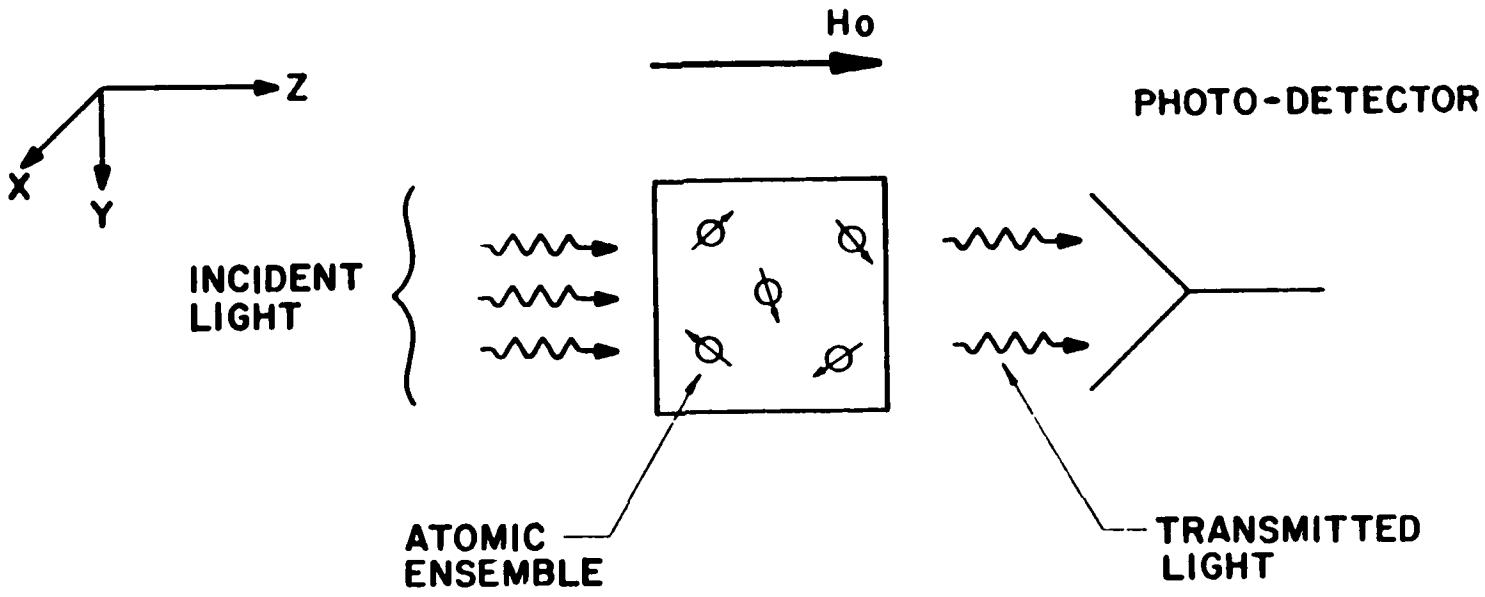

FIG. 2

OPTICAL PUMPING SYSTEM

B54542-PRL

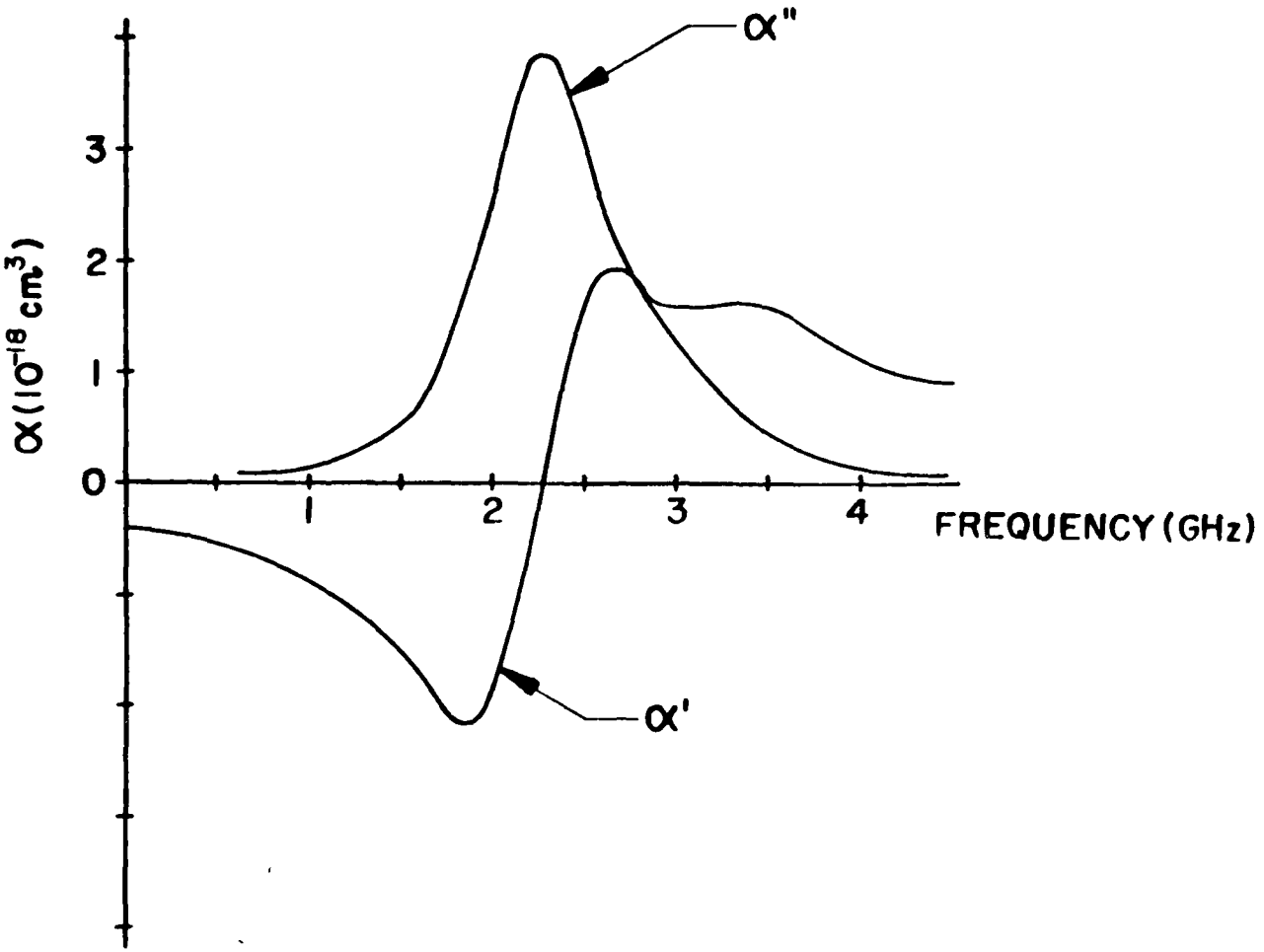

FIG. 3

D₁ POLARIZABILITY OF Rb^{87} NEAR RESONANCE

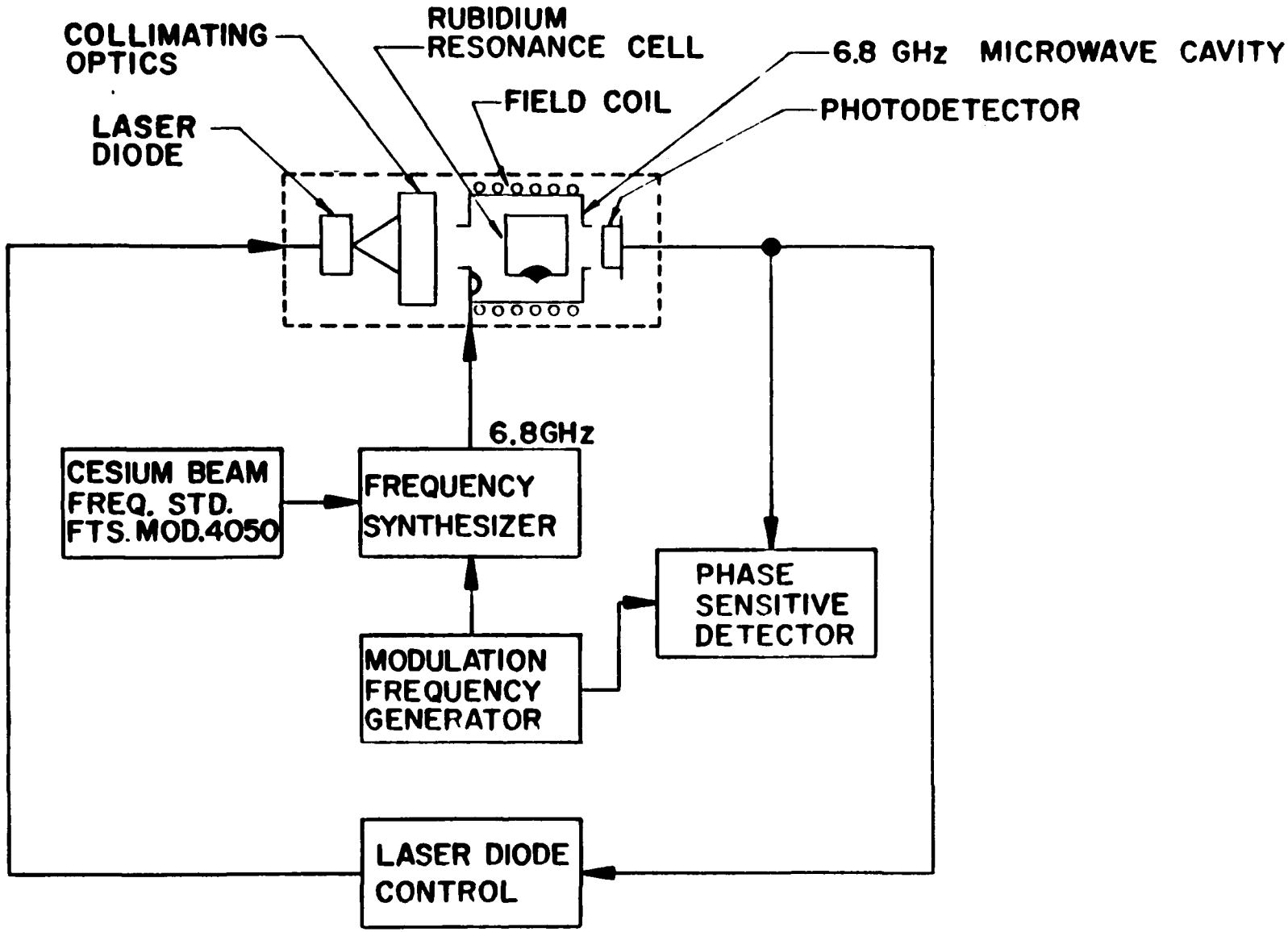

FIG. 4

EXPERIMENTAL APPARATUS

150 MHz

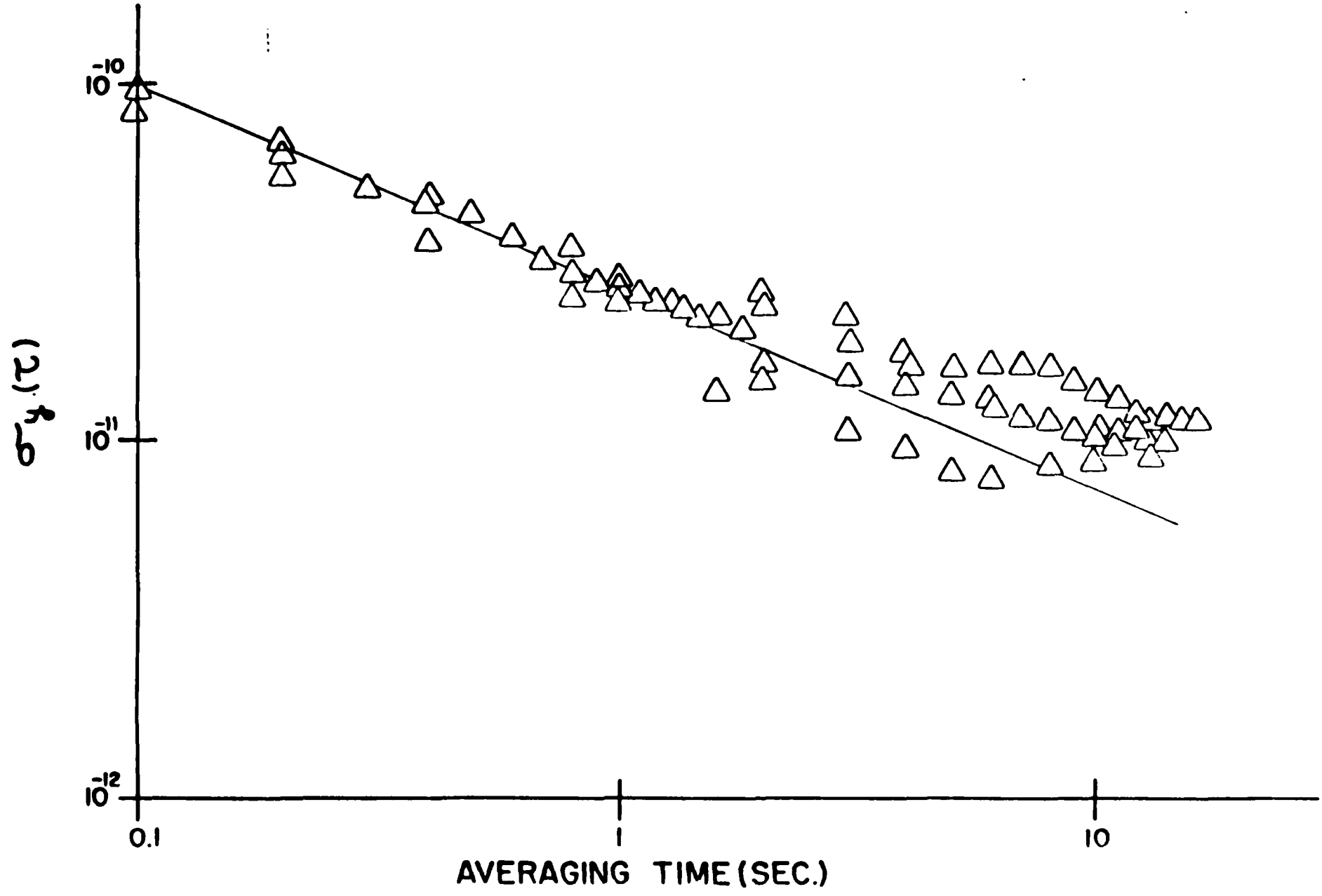

B54546-PRL

FIG. 6

ALLAN VARIANCE OF LASER DIODE SYSTEM

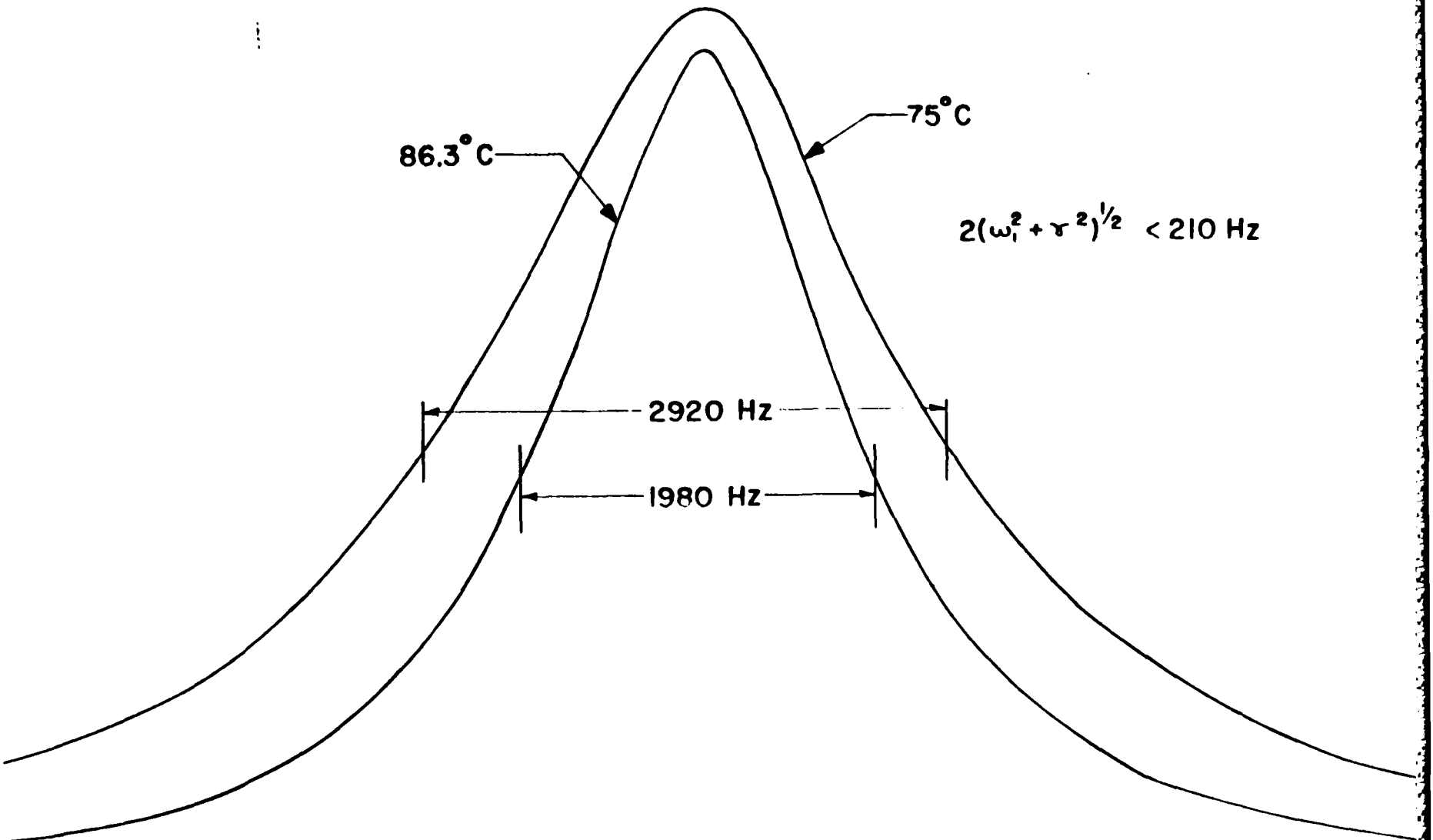

FIG. 7

MEASURED HYPERFINE RESONANCE LINES

B54547-PRL

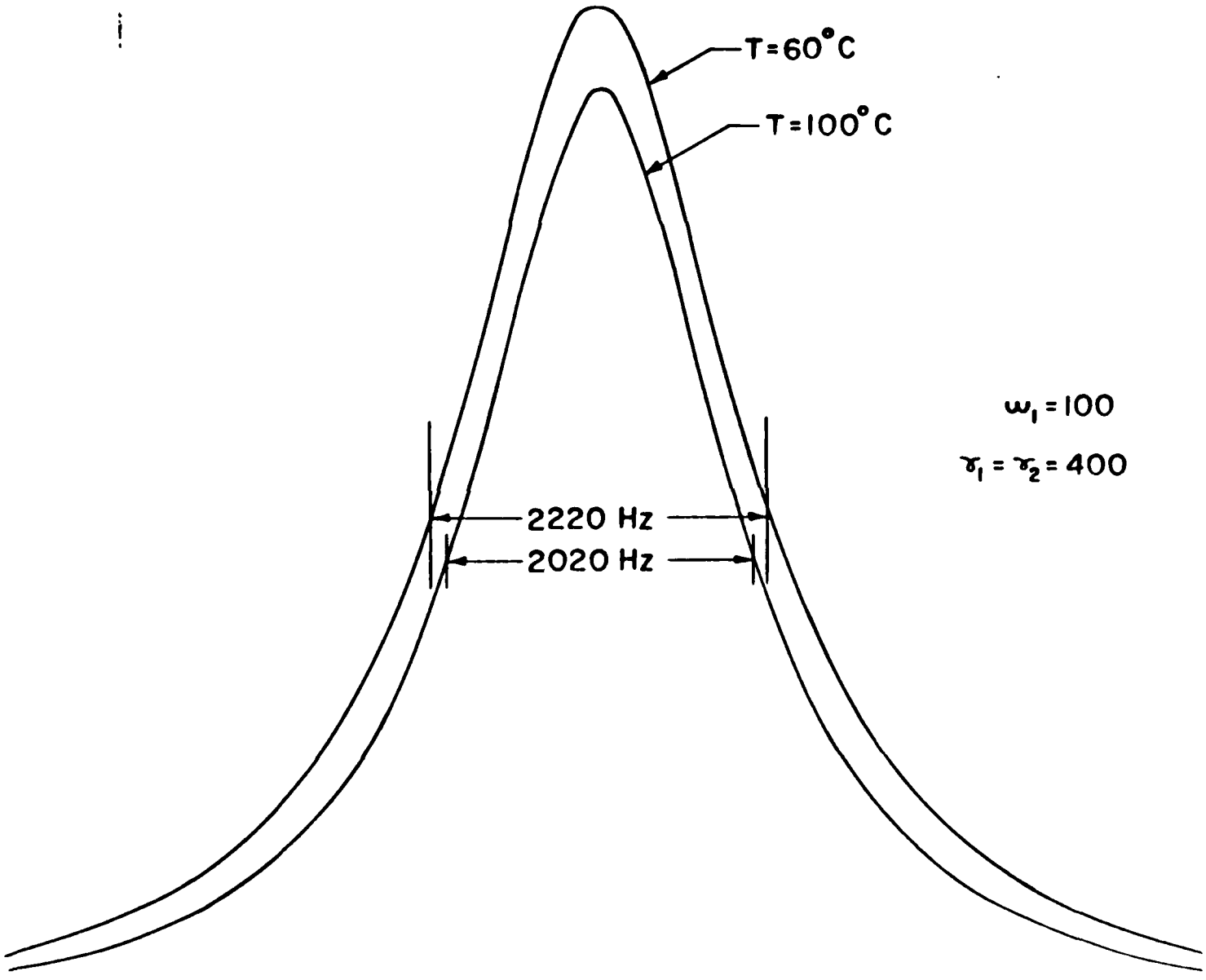

FIG. 8

THEORETICAL HYPERFINE RESONANCE LINES

B54546-PRL

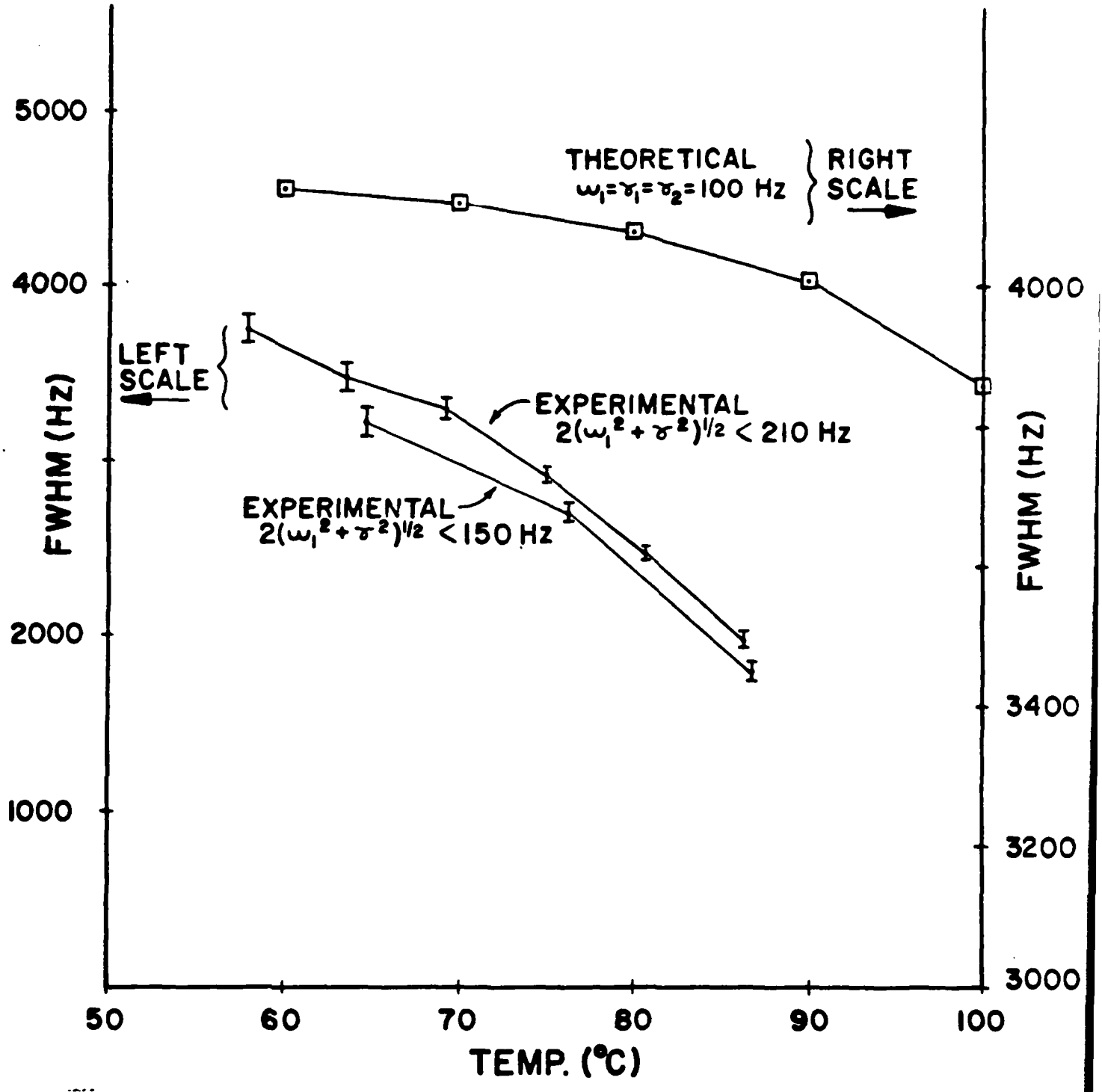

FIG. 9

LINEWIDTH vs TEMPERATURE

BS4548-PRL

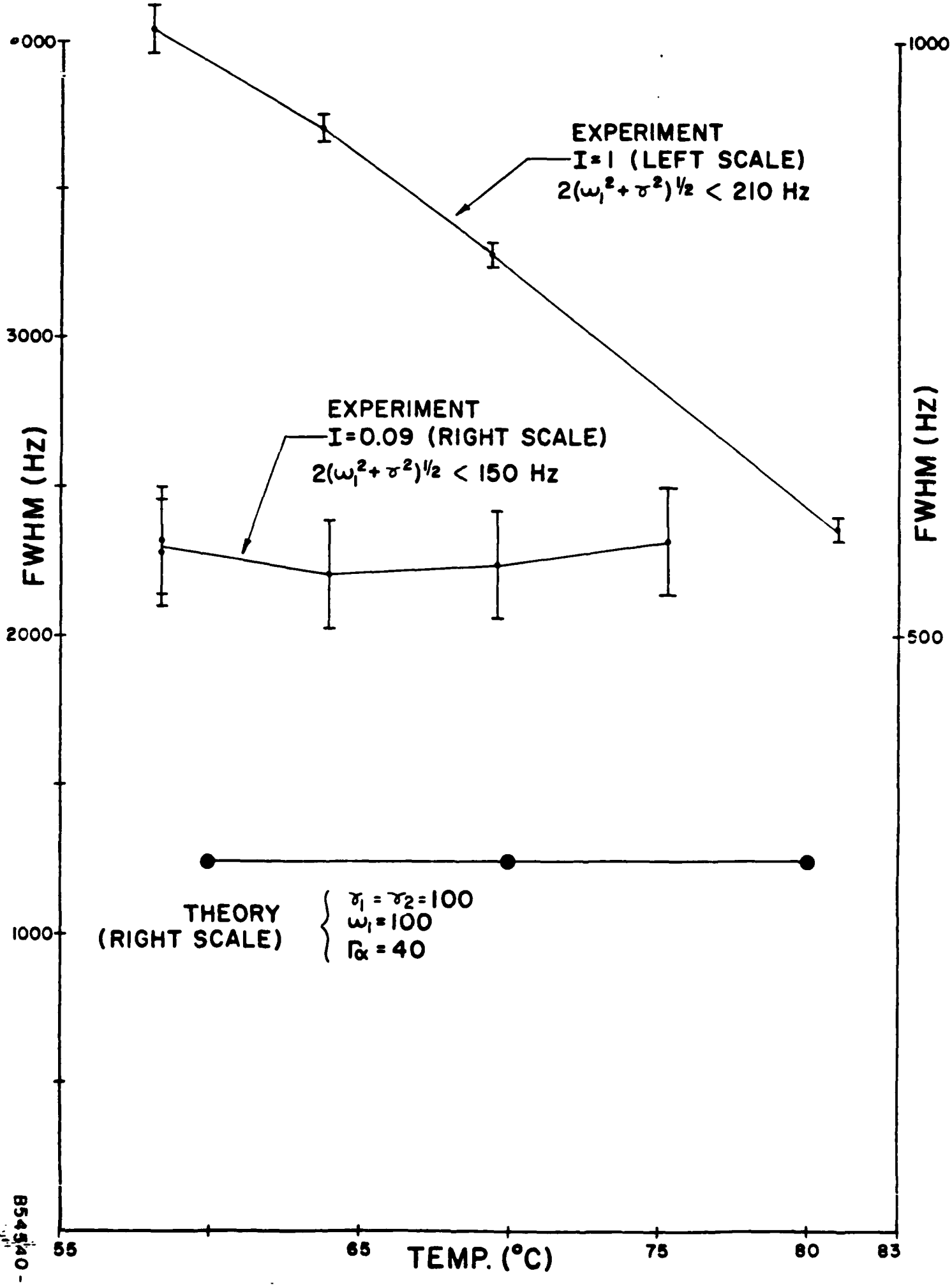
4000
3000
2000
1000
FWHM (HZ)
1000
500
FWHM (HZ)
EXPERIMENT
I=1 (LEFT SCALE)
2(ω1² + σ²)½ < 210 Hz
EXPERIMENT
I=0.09 (RIGHT SCALE)
2(ω1² + σ²)½ < 150 Hz
THEORY
(RIGHT SCALE)
σ1 = σ2 = 100
ω1 = 100
Γα = 40
55
65
75
80
83
TEMP. (°C)
85454-0

END

FILMED

1-86

DTIC